Wwc2 is a novel cell division/fate regulator during preimplantation mouse development and oogenesis

Giorgio Virnicchi[1*], Pablo Bora[1], Lenka Gahurová[1], Andrej Šušor[2] and Alexander William Bruce[1*]

[1] Laboratory of Early Mammalian Developmental Biology (LEMDB),
Department of Molecular Biology & Genetics,
Faculty of Science,
University of South Bohemia,
Branišovská 31,
370 05 České Budějovice (Budweis),
CZECH REPUBLIC.

[2] Laboratory of Biochemistry and Molecular Biology of Germ Cells,
Institute of Animal Physiology and Genetics,
Czech Academy of Sciences, Rumburská 89,
277 21 Liběchov,
CZECH REPUBLIC.

[*]correspondence; A.W.B. awbruce@prf.jcu.cz & G.V. giorgio.virnicchi@gmail.com
Tel: +420387772291
Fax: +42038777226 (not confidential)

Total charcter count:

Running title: *Wwc2*: novel cell division/fate regulator

ABSTRACT

Derivation mouse blastocysts (E4.5) marks the end of the preimplantation period, whereby the earliest developmental events are manifest in regulated cell cleavage divisions and formation of three distinct cell lineages. We report targeted dysregulated expression of the *Wwc2* gene, an ill characterised paralog of the Hippo-signalling activator *Kibra/Wwc1*, is specifically associated with cell autonomous deficits in embryo cell number and gross division abnormalities/phenotypes; typified by imbalanced daughter cell chromatin segregation. This early mitotic regulatory role is conserved during mouse oocyte meiotic maturation, whereby *Wwc2* dysregulation blocks progress to the fertilisation competent stage of meiosis II metaphase arrest, with attendant spindle defects and failed Aurora kinase A (AURKA) activation. *Wwc2* specific cell division phenotypes, each occurring in the absence of centrosomes, are fully revertible by expression of recombinant HA-epitope tagged WWC2 and restores activated AURKA levels, in embryos and oocytes, respectively. Additionally, clonal dysregulation implicates *Wwc2* in maintaining the pluripotent late blastocyst stage epiblast lineage. Thus, *Wwc2* is a novel regulator of meiotic and early mitotic cell divisions, and subsequently mouse blastocyst cell fate.

Keywords: cell division/ meiosis/ mitosis/ mouse oocyte/ preimplantation embryo.

INTRODUCTION

During the 4.5 days after fertilisation of mouse metaphase II arrested secondary (MII) oocytes, a series of asynchronous cell cleavage divisions generates blastocysts capable of uterine implantation. Such blastocysts comprise three distinct cell lineages; an outer-residing, differentiating and apical-basolaterally polarised epithelium called the trophectoderm (TE – a progenitor of placental tissue), differentiating primitive endoderm (PrE – precursors of the yolk sac), represented as a polarised superficial mono-layer of inner-cell mass (ICM) cells in contact with the fluid filled cavity and the pluripotent epiblast (EPI – progenitors of subsequent foetal tissue), found completely encapsulated within the ICM (comprehensively reviewed (Chazaud & Yamanaka, 2016, Frum & Ralston, 2015, Mihajlovic & Bruce, 2017, Rossant, 2016, Rossant, 2018, White, Zenker et al., 2018)). Amongst uncovered molecular mechanisms governing the emergence of such blastocyst cell fates is the differential regulation of Hippo-signalling pathway (originally identified in *Drosophila* as a cell proliferation and tissue growth/size regulating pathway but now implicated in varied developmental/pathological paradigms (Davis & Tapon, 2019)). Specifically, it is within the encapsulated and apolar inner-cells of the nascent ICM that active, adherens junction (AJ) localised, Hippo-signalling centres form and potentiate the core kinases LATS1/2 (aided by the essential activator AMOT) to phosphorylate the transcriptional cofactors effectors YAP and WWTR1/TAZ (collectively referred to here as YAP) (Cockburn, Biechele et al., 2013, Leung & Zernicka-Goetz, 2013, Nishioka, Inoue et al., 2009). Such YAP phosphorylation prevents YAP nuclear accumulation and ensures members of the TEA-domain containing transcription factors (specifically TEAD4 in this context) are unable to activate TE-specific genes (*e.g. Cdx2* or *Gata3*) (Nishioka et al., 2009). Conversely, AJ localised Hippo-pathway activation at the basolateral membranes of polarised outer-cells is actively suppressed via AMOT protein sequestration to the cell contactless apical pole, permitting unphosphorylated YAP to enter the nucleus and molecularly endow TEAD4 to appropriately transcriptionally activate TE-related gene expression. It is therefore, the initial inheritance, or otherwise, of an apical pole enriched in apical polarity factors (*e.g.* aPKC-Par complex) that defines whether dividing 8-cell (E2.5) or outer 16-cell (E3.0) stage progeny blastomeres, respectively suppress or activate Hippo-signalling and hence exhibit pluripotency (as an inner-cell) or initiate TE differentiation (as an outer-cell). Indeed, experimental strategies to disrupt outer-cell apical-basolateral polarity (Alarcon, 2010, Hirate, Hirahara et al., 2013, Kono, Tamashiro et al., 2014, Mihajlovic & Bruce, 2016), or abrogate *Tead4* expression (Mihajlovic, Thamodaran et al., 2015, Nishioka, Yamamoto et al., 2008, Yagi, Kohn et al., 2007), result in failed outer-cell TE specification and ectopic ICM pluripotency-related marker gene expression (reviewed (Hirate, Hirahara et al., 2015, Sasaki, 2017)). However, interestingly YAP enabled TEAD4 complexes simultaneously suppress pluripotent gene expression (*e.g. Sox2*) in derived outer-cells (Frum, Murphy et al., 2018, Wicklow, Blij et al., 2014) and also act to prevent precocious *Sox2* expression prior to the 16-cell stage (Frum, Watts et al., 2019). Consistently, experimentally activated Hippo-signalling (*i.e.* via LATS1/2 over-expression, to antagonise YAP-TEAD4 formation) can potentiate *Sox2* expression (even in outer-cells) by the 32-cell/ early blastocyst stage (Wicklow et al., 2014), but eventual EPI specification by the late blastocyst stage, actually requires subsequent YAP translocation into the nucleus; an inherently heterogeneous process causing competitive apoptotic elimination of EPI progenitors exhibiting reduced naïve pluripotency-related gene expression (correlated with low nuclear YAP levels) (Hashimoto & Sasaki, 2019). Thus collectively, these data illustrate the emerging integral nature of Hippo-signalling in regulating key cell fate events in early mouse

embryogenesis and suggests roles for other, particularly upstream and potentially novel, factors capable of functionally interacting with core Hippo-pathway machinery.

The *Drosophila* WW-domain and C2-domain containing (WWC-domain) gene *Kibra* was initially reported as a positive regulator of Hippo-signalling, causing phosphorylation of the fly orthologue of mammalian LATS1/2 (*i.e.* warts/Wts) in a number of tumour suppressor/cell proliferation screens (Baumgartner, Poernbacher et al., 2010, Genevet, Wehr et al., 2010, Yu, Zheng et al., 2010); a role subsequently confirmed in mammalian cells (Xiao, Chen et al., 2011a). Unlike in *Drosophila*, tetrapod genomes typically encode three WWC-domain paralogs, called *KIBRA/WWC1*, *WWC2* and *WWC3*, although the *Mus musculus* genome has lost the would be *Wwc3* gene due to an evolutionarily recent chromosomal deletion. The paralogous human WWC-domain proteins are highly conserved, cable of homo- and hetero-dimerisation, can all activate Hippo-signalling (causing LATS1/2 and YAP phosphorylation) in inducible cell line models and cause the Hippo-related *Drosophila* 'rough-eye' phenotype, caused by reduced cell proliferation, when over-expressed in the developing fly eye (Wennmann, Schmitz et al., 2014). Despite a comparatively large pan-model KIBRA-related Hippo-pathway activator literature, the roles of WWC2/3 are considerably understudied and restricted to limited reports consistent of tumour suppressor function in specific cancers (*e.g.* hepatocellular carcinoma (Zhang, Yan et al., 2017) and epithelial-mesenchymal lung cancers (Han, Kremerskothen et al., 2018)). Moreover, there exist no reports of a functional role of any WWC-domain gene/protein during mammalian preimplantation development, regardless of the proven and crucial importance of differential regulation of the Hippo-signalling pathway. (Sasaki, 2017).

Ovulated secondary mouse MII oocytes arise from subpopulations of primary oocytes, arrested in the dictyate stage of prophase of meiosis I (MI) since prenatal development, stimulated by maternal reproductive hormones to re-enter and complete meiosis I (reviewed (Sanders & Jones, 2018)). In addition to ensuring both the necessary growth required to support later embryonic development and expression of gene products required to execute meiosis, meiotic maturation ensures replicated chromosomal bivalents are appropriately resolved and faithfully segregated between the first polar body and a developmentally competent secondary MII oocyte (itself capable of faithfully segregating sister chromatids between a second polar body and the resulting zygote, post-fertilisation). Failure to precisely segregate chromosomes, resulting in egg and/or zygotic aneuploidy, has severe and usually terminal consequences for embryonic development, with aneuploidy attributable to the human female germline recorded as the leading single cause of spontaneously aborted pregnancy (Hassold & Hunt, 2001, Nagaoka, Hassold et al., 2012). An extensive literature covering the varied and integrated molecular mechanisms underpinning the germane segregation of homologous chromosomes during MI exists; ranging across meiotic cell-cycle resumption, germinal vesicle (GV/nuclear envelope) breakdown, meiotic spindle assembly, spindle microtubule-kinetochore attachment, chromosomal congression, functioning of the spindle assembly checkpoint (SAC), regulation of the anaphase promoting complex/cyclosome (APC/C) and regulation of cytokinesis/polar body generation (see comprehensive reviews (Bennabi, Terret et al., 2016, Mihajlovic & FitzHarris, 2018, Mogessie, Scheffler et al., 2018, Namgoong & Kim, 2018, Sanders & Jones, 2018)). As with all mammals, and unlike most mitotic somatic cells, meiotic spindle formation in primary mouse oocytes occurs in the absence of centrioles/centrosomes and is initiated in the vicinity of condensing chromosomes from coalescing microtubule organising centres (MTOCs) and further stabilised by chromosome derived RAN-GTP gradients that respectively promote and inhibit microtubule polymerisation and destabilisation (Bennabi et al., 2016, Gruss, 2018, Mogessie et al., 2018, Namgoong & Kim, 2018, Severson, von

Dassow et al., 2016). Unlike other mammalian developmental systems, the transition from MTOC initiated spindle formation to centrosomal control in mice only occurs by the mid-blastocysts stage, when centrosomes appear *de novo* ((Courtois, Schuh et al., 2012)); contrasting with other mammals (*e.g.* humans) were fertilising sperm provide a founder centrosome that ensures the first mitotic spindle is assembled centrosomally (Sathananthan, Kola et al., 1991, Schatten & Sun, 2009). Thus, formation and functioning of the first meiotic, and somewhat uniquely, early mitotic spindles in mice are subject to non-centrosomal based regulation. Amongst known key regulators of spindle dynamics are the conserved Aurora-kinase family proteins (AURKA, AURKB & AURKC, collectively referred to here as AURKs) that all exhibit germ cell and early embryonic expression (AURKC is not expressed in other somatic cells (Li, Wang et al., 2017)). During meiosis, AURKs impart important regulatory roles in spindle formation/ organisation, MTOC clustering, chromosome condensation and alignment, plus correct microtubule-kinetochore attachment, chromosomal cohesion and cytokinesis in mitosis (reviewed in (Nguyen & Schindler, 2017)). Specifically, AURKA protein is essential for MI progression (Saskova, Solc et al., 2008) and is continually localised with MTOCs and MI/ MII spindle poles, regulating clustering and initiating microtubule nucleation/dynamics, throughout meiosis (Nguyen, Drutovic et al., 2018, Nguyen & Schindler, 2017, Solc, Baran et al., 2012, Swain, Ding et al., 2008); with similar roles in post-fertilisation zygotes (Kovarikova, Burkus et al., 2016).

We report specific disruption of *Wwc2* expression in mouse embryo blastomeres results in cell autonomous division and cleavage phenotypes, yielding blastocysts with fewer overall cells, and is associated with mis-segregated chromosomes and defective cytokinesis (not replicated by targeted dysregulation of *Kibra*). Similar cell division phenotypes are also associated with impaired *Wwc2* expression in meiotically maturating mouse primary oocytes and are coincident with profound spindle defects and blocked activation/phosphorylation of AURKA. Observed oocyte and embryo cell division phenotypes are rescuable by the expression of epitope-tagged recombinant WWC2 protein, that in embryos localises with mid-body structures and is able to restore appropriate cellular contribution to the pluripotent EPI, which is normally lacking following dysregulation of *Wwc2* expression.

157 **RESULTS**

158

159 **WWC-domain containing genes are expressed in preimplantation mouse embryos**

160 In the context of the central role of Hippo-signalling in mouse preimplantation embryo development (Sasaki,
161 2017), we investigated the potential regulatory role of WWC-domain containing genes (*i.e. Kibra* and *Wwc2* in mice
162 (Wennmann et al., 2014)) in blastocyst formation. Accordingly, we assayed *Kibra* and *Wwc2* mRNA expression in
163 preimplantation mouse embryos microinjected with non-specific control dsRNA or constructs specific for each gene
164 (Fig. 1a). Stable levels of *Kibra* and *Wwc2* transcripts were readily detectable at both 8- (E2.5) and 32-cell (E3.5)
165 stages, with normalised *Wwc2* expression twice as abundant as *Kibra*. Each transcript level could be robustly reduced
166 using dsRNA mediated global knockdown at both assayed stages (note, a lack of available antibodies prevented
167 protein expression assays). We next assayed for overt developmental defects associated with individual or combined
168 *Kibra*/*Wwc2* knockdown by microinjecting dsRNA(s) in one blastomere of 2-cell (E1.5) stage embryos, culturing to
169 the late blastocyst (E4.5) stage and counting total cell number (Fig. 1b). *Kibra* gene knockdown had no significant
170 effect on total cell number, or embryo morphology (versus control dsRNA), but a severe attenuation in cell number
171 when targeting *Kibra* and *Wwc2* transcripts in combination was observed. Interestingly, this defect was statistically
172 indistinguishable from the group of embryos microinjected with *Wwc2* dsRNA alone, indicating sole knockdown of
173 the *Wwc2* paralog was sufficient to induce the observed phenotype (note, *Kibra* mRNA levels were unaffected by
174 *Wwc2* dsRNA by the 8-cell/E2.5 stage, whereas *Wwc2* transcripts were robustly reduced, confirming *Wwc2* dsRNA
175 specificity – Fig. 1a and supplementary Fig. S1). Repetition of the *Wwc2* knockdown, in a fluorescently marked clone
176 (whereby rhodamine conjugated dextran beads/ RDBs were co-injected with *Wwc2* dsRNA) confirmed reduced cell
177 numbers as early as the 16-cell (E3.0) stage, specifically within the marked clone that itself exhibited reduced
178 contribution to the initial inner-cell/ ICM founding population (Fig. 1c). Accordingly, we decided to focus our further
179 investigations on the overt cell number deficit phenotype associated with *Wwc2* knockdown.

180

181 **Reduced embryo cell numbers caused by *Wwc2* knockdown are associated with defective cell division.**

182 Although the utilised *Wwc2* dsRNA was carefully designed to avoid off target effects (with specific respect
183 to *Kibra* expression, Figs. 1a & S1), we sought to phenocopy our observations using an siRNA mediated approach
184 (targeting an alternative region of the *Wwc2* mRNA – Fig. S1); thus, providing added confidence to our initial
185 observations and affording the option of phenotypic rescue, by expressing recombinant siRNA-resistant *Wwc2*
186 mRNA. Figure 2 confirms the selected *Wwc2* siRNA near completely eliminated detectable *Wwc2* transcripts, after
187 global knockdown, in 32-cell (E3.5) stage blastocysts. Moreover, subsequent to the microinjected 2-cell (E1.5) stage,
188 an assay of total cell number at all cleavage stages up to the late blastocyst (E4.5) stage revealed an accumulative
189 and statistically robust deficit beginning after the 8-cell (E2.5) stage (Fig. 2c). Indeed, from the equivalent 8-cell
190 (E2.5) to 32-cell (E3.5) stages (judged by control embryo development), total cell number did not significantly
191 increase in *Wwc2* knockdown embryos but did start to increase during the blastocyst maturation period (32- to >64-
192 cell, as judged in control embryo groups; *i.e.* E3.5 – E4.5 stages). It was not unusual for the *Wwc2* knockdown
193 embryos to initiate cavitation (not shown). We also assayed if the *Wwc2* siRNA phenotype was cell autonomous by
194 creating RDB marked *Wwc2* specific siRNA knockdown clones (comprising 50% of the embryo – Fig. S2). As
195 expected, we observed a statistically significant *Wwc2* siRNA mediated deficit in cell number within the

196 microinjected clone (versus the non-microinjected sister clones and the equivalent microinjected clone in control
197 siRNA embryos) at all stages, from the 8-cell (E2.5) to the late blastocyst (E4.5). However, we did not observe
198 significant differences between control and *Wwc2* knockdown groups in the number of cells within the non-
199 microinjected clone (with the exception of the 32-cell (E3.5) stage where there was an average of 2.3 fewer cells in
200 the *Wwc2* knockdown group). These data support a novel and cell autonomous role for *Wwc2* in ensuring appropriate
201 cell number during preimplantation mouse embryo development. Whilst assaying cell numbers, we observed a
202 number of nuclear/chromatin morphological abnormalities within *Wwc2* knockdown embryos, not evident in control
203 embryos. Illustrative examples, at the equivalent of the 32-cell (E3.5) stage are provided (Fig. 3b) and were
204 categorised as; 'abnormal nuclear morphology' (including that typical of persistent 'association with the mid-body'),
205 associated with 'cytokinesis defects' (typified by bi-nucleated cells) or coincident with 'multiple or micronuclei'.
206 Accordingly, we calculated the frequencies by which each, or a composite of, the stated abnormalities were observed
207 (compared to control siRNA conditions) at each assayed cleavage stage; defined per embryo (in at least one
208 blastomere) or per individual assayed cell (Fig. 3c). Except from a single incidence of an early blastocyst stage cell
209 exhibiting a single micronucleus, no other abnormalities were observed in any control siRNA microinjected embryo,
210 at any developmental stage. Conversely, abnormally shaped nuclei were present in over a quarter of *Wwc2*
211 knockdown embryos at the 8-cell (E2.5) stage and were found in all assayed embryos by the equivalent late blastocyst
212 (E4.5) stage. A similar trend, from the 16-cell (E3.0) stage, was observed in relation to multiple/micronuclei. Despite
213 being less prevalent, cytokinetic defects affected nearly a quarter of *Wwc2* knockdown embryos by the late blastocyst
214 (E4.5) stage. Indeed, all *Wwc2* knockdown embryos exhibited one or more defect, in at least one cell, by the mid-
215 blastocyst (E4.0) stage, with the collective defects (excluding cytokinesis/bi-nucleation) first arising in just over a
216 quarter of 8-cell stage (E2.5) embryos. When we analysed the same phenotypes on the level of each individually
217 assayed blastomere, we found that just over a quarter of cells were affected by the late blastocyst (E4.5) stage;
218 however, it should be noted that such embryos comprised a much smaller average of overall cells, versus control
219 siRNA groups (*i.e.* 31.3±3.0 against 87.0±3.8 - Fig. 2c). Hence, our collective interpretation is *Wwc2* knockdown in
220 cleavage stage mouse embryos is associated with cell autonomous division defects that contribute to embryos with
221 progressively fewer constituent blastomeres as preimplantation development proceeds past the 8-cell stage; invoking
222 a role for *Wwc2* in regulating appropriate cell division/ mitosis in blastomeres of the early mouse embryo.
223
224 ***Wwc2* mRNA depletion in primary (GV) oocytes impairs meiotic maturation.**
225 We next asked the question whether a similar knockdown of *Wwc2* expression in meiosis I arrested germinal
226 vesicle (GV) stage primary mouse oocytes would elicit any cell cycle defects during maturation to the MII stage,
227 particularly because both mouse embryonic blastomere cleavage divisions and meiotic oocyte maturation represent
228 paradigms of cell division that occur in the absence of centrosomes/centrioles (Bennabi et al., 2016, Coelho, Bury et
229 al., 2013, Courtois et al., 2012, Gruss, 2018, Mogessie et al., 2018, Namgoong & Kim, 2018, Severson et al., 2016).
230 We first observed abundant *Wwc2* transcripts in GV and MII oocytes (plus zygotes), that show evidence of becoming
231 cytoplasmically poly-adenylated and hence more likely to be translated as required functional proteins (Salles,
232 Darrow et al., 1992), between the GV and MII stages (as revealed using alternative, oligo-dT versus random hexamer,
233 cDNA synthesis priming strategies - Fig. 4a). Indeed, consultation of our previously published assay of meiotically
234 maturing oocyte polysome associated transcripts (Koncicka, Tetkova et al., 2018) supported this interpretation (~40%

235 polysome association; Fig. 4b). We next confirmed our siRNA construct could elicit robust *Wwc2* transcript
236 knockdown in microinjected GV oocytes, that had been blocked from re-entering meiosis I (using a cAMP/cGMP
237 phosphodiesterase inhibitor, 3-isobutyl-1-methylxanthine/ IMBX) and then permitted them to *in vitro* mature (IVM)
238 to the MII equivalent stage (Fig. 4c & d). Such oocytes were fixed and immuno-fluorescently stained for α-Tubulin
239 (plus DAPI DNA stain), to assay for potential division phenotypes. In our two control conditions (*i.e.* non-
240 microinjected or control siRNA microinjected oocytes) >90% of GV oocytes matured to the MII arrested stage,
241 typified by an extruded polar body (PB1) and metaphase II arrested spindle. However, in the *Wwc2* knockdown
242 group, the successful IVM rate was reduced to 8.6% and oocytes presented with various arrested phenotypes (lacking
243 PB1) that we categorised by the presence of metaphase I meiotic spindles (*i.e.* -PB1 +MI spindle; 42.9%, note such
244 spindles typically failed to migrate to the oocyte cortex), spindle-like structures with mis-aligned or dispersed
245 chromosomes (-PB1 +spindle defect; 22.9%) or a non-nuclear membrane enveloped ball of chromatin (-PB1+ultra-
246 condensed chromatin; 25.7%), collectively indicative of severely impaired segregation of bivalent chromosomes
247 during a defective meiosis I (Fig. 4e). Despite, permitting assayed GV oocytes to meiotically mature for 18 hours,
248 we wanted to confirm if the observed *Wwc2* knockdown phenotypes would persist or resolve if provided with
249 increased time (possibly indicative of delayed rather than blocked meiotic progression). We repeated the *Wwc2*
250 knockdown experiment allowing an extended IVM period of 24 hours. However, no increased frequency of MII
251 arrested oocyte generation was observed; rather *Wwc2* mRNA depleted oocytes either remained blocked in meiosis
252 I or unsuccessfully attempted to segregate their chromosomes, without undergoing cytokinesis (Fig. S3).
253
254 ***Wwc2* specific oocyte meiotic maturation phenotypes are associated with failed Aurora kinase-A (AURKA)**
255 **activation.**
256 It is reported that activated/phosphorylated Aurora kinase-A (p-AURKA: p-Thr288) is required to initiate
257 acentriolar/MTOC mediated spindle assembly in mouse oocytes and that *Aurka* knockdown phenotypes resemble
258 those observed here for *Wwc2* knockdown (Bury, Coelho et al., 2017). Thus, we hypothesised the observed meiotic
259 maturation phenotypes may be associated with impaired levels of activated p-AURKA. A western blot analysis of
260 staged maturing oocytes confirmed characteristically low levels of p-AURKA in GV oocytes, that robustly increased
261 with the appearance of the first meiotic spindle (during MI) and were maintained with the formation of the second
262 meiotic spindle (in MII arrest; Fig. 5b & (Nguyen & Schindler, 2017, Saskova et al., 2008)); a trend replicated in
263 control siRNA microinjected GV (assayed after 18 hour incubation in IMBX) and MII (after 16 hours post-IBMX
264 removal) oocytes (note, the specificity of the anti-p-AURKA antibody used was additionally confirmed; Fig. S4).
265 However, in the *Wwc2* siRNA microinjected group, we were not able to detect p-AURKA at either the equivalent
266 GV or MII temporal stages. Moreover, we were also unable to detect p-AURKA immuno-reactivity localised to the
267 poles of any spindles or spindle-like structures formed in *Wwc2* knockdown oocytes, in stark contrast to that observed
268 on MII arrested spindles in control oocytes (Fig. 5c). Thus, these results confirmed a failure to activate AURKA
269 under conditions of experimentally diminished *Wwc2* transcript expression that is associated with profound meiotic
270 oocyte maturation cell division defects.
271 Despite obtaining consistent *Wwc2*-specifc RNAi cell division phenotypes using distinct dsRNA/siRNA
272 constructs in both mouse oocytes and preimplantation embryos and their careful design aimed to avoid potential off-
273 target effects or cross reactivity with paralogous *Kibra* mRNA (Figs. 1 and S1), we sought to further experimentally

274 verify the identified novel role of *Wwc2* during primary oocyte meiotic maturation. Accordingly, we derived a
275 recombinant and N-terminally HA-epitope tagged *Wwc2* mRNA construct (*HA-Wwc2*) that had been specifically
276 mutated within the siRNA complementary sequence (yet preserving a redundant sequence of amino acid codons; see
277 Fig. S5) to block recognition and hence remain available for translation in *Wwc2* siRNA microinjected oocytes. We
278 repeated our described IVM assay (assaying at multiple time-points) and found that co-microinjection of *HA-Wwc2*
279 mRNA and *Wwc2* siRNA led to a robust rescue the maturation phenotypes caused by *Wwc2* siRNA microinjection
280 alone (*i.e.* MII arrested oocytes at 16 hours post-IBMX; control siRNA – 81.8%, *Wwc2* siRNA - 8.7% & *HA-Wwc2*
281 mRNA plus *Wwc2* siRNA – 76.0%). Moreover, the progression of the observed rescue through recognisable oocyte
282 maturation stages was in-step with that of control siRNA microinjected oocytes (as measured at 1, 6, 12 and 16 hours
283 post-IBMX removal; Fig. 6d). Consistently we also found co-microinjection of the rescue *HA-Wwc2* mRNA
284 construct was coincident with reappearance of activated p-AURKA protein (Fig. 6e), that was also detected in
285 proximity to forming or matured MI/MII stage meiotic spindles (Fig. S6). Collectively, these data confirm a novel
286 role for *Wwc2* in regulating appropriate chromosome segregation and cell division during mouse primary oocyte
287 meiotic maturation (strongly associated with activation of the acentriolar/MTOC mediated spindle forming
288 meiotic/mitotic kinase AURKA) that displays functional conservation with that observed in the similarly
289 acentrosomal mitotic cleavages of preimplantation stage embryonic blastomeres.
290
291 **siRNA mediated *Wwc2* knockdown affects blastocyst cell fate derivation.**
292 As described, cell number deficit/defective cell division phenotypes were first evident in global siRNA
293 mediated *Wwc2* knockdown embryos around the 8- to 16-cell stage (Figs. 2 & 3). Moreover, clonal dsRNA mediated
294 *Wwc2* knockdown was specifically associated with reduced inner-cell clone numbers (Fig. 1c). As the transition from
295 the 8- to 16-cell stage, represents the first developmental point constituent embryonic cells are overtly distinct, both
296 in terms of intra-cellular apical-basolateral polarity and relative spatial allocation, with consequences for ultimate
297 blastocyst cell fate (*i.e.* comprising polarised outer-cells that can give rise to both TE and further inner-cells, plus
298 apolar inner ICM progenitors (Johnson & Ziomek, 1981)), we assayed if clonal *Wwc2* knockdown altered TE versus
299 ICM cell fate by the early blastocyst (E3.5) stage. The need to assay the first cell fate decision, in this context, was
300 further reinforced by cited precedents implicating *Kibra,* and hence by association its paralog *Wwc2*, in activating
301 Hippo-signalling in flies and mammals (Baumgartner et al., 2010, Genevet et al., 2010, Wennmann et al., 2014, Xiao
302 et al., 2011a, Yu et al., 2010), a pathway itself central to TE /ICM specification in mouse preimplantation embryos
303 (Sasaki, 2017). Accordingly, we created stably marked clones of *Wwc2* knockdown and control cells (by expressing
304 recombinant GAP43-GFP as an injection membrane marker) and assayed expression of the Hippo-sensitive TE
305 marker protein CDX2 (Strumpf, Mao et al., 2005) (Fig. 6). Control siRNA treated embryos developed appropriately
306 to yield 32-cell (E3.5) stage blastocysts consisting an average of 59% outer (CDX2 positive) and 41% inner (CDX2
307 negative) cell populations, with a statistically equal contribution from each clone (*i.e.* either control siRNA
308 microinjected or non-microinjected derived). As expected, *Wwc2* siRNA microinjected embryos comprised
309 significantly fewer cells with the microinjected clone also characterised by the previously observed abnormal nuclear
310 morphologies and a robustly significant impaired contribution to the ICM; on average 1.6±0.2 cells versus 6.8±0.3
311 in the non-microinjected clone (or 7.3±0.4 or 7.4±0.3 in the respective clones of control siRNA microinjected
312 embryos). Clonal TE contribution was also significantly impaired but to a much lesser degree and the potential TE

313 deficit was compensated by an increased contribution from the corresponding non-microinjected clone. We also
314 observed a small outer-cell population of *Wwc2* knockdown clones that failed to express CDX2 (~20%; not observed
315 in control embryos) with the remaining outer-cells often exhibiting comparatively reduced CDX2 immunoreactivity,
316 when compared to both the non-microinjected clone or either clone in the control siRNA microinjected groups
317 (concurrently immuno-stained and imaged using identical protocols; Fig. 6b). However, no ectopic CDX2 expression
318 within inner-cells of the *Wwc2* knockdown clone was observed and the non-microinjected clone appropriately only
319 expressed CDX2 in outer-cells. Therefore, consequent to clonal *Wwc2* knockdown, the overall percentage make up
320 of outer and inner-cells was skewed in favour of outer TE (largely CDX2 positive – 72%) over ICM (exclusively
321 CDX2 negative - 28%). These results suggest that the required outer-cell Hippo-pathway suppression (to specify TE)
322 and inner-cell activity (to prevent TE differentiation and promote pluripotency) are predominantly intact within the
323 *Wwc2* knockdown clone, although maintenance of TE specification/ differentiation in outer-cells is modestly
324 impaired. Therefore, endogenous *Wwc2* is unlikely to function as a critical Hippo-signalling pathway (*i.e.* LATS1/2)
325 regulator (as implied by previous *Kibra/KIBRA* related reports demonstrating a role in Warts/LATS1/2
326 phosphorylation/activation in *Drosophila* and mammalian cells (Baumgartner et al., 2010, Genevet et al., 2010,
327 Wennmann et al., 2014, Xiao et al., 2011a, Yu et al., 2010)) in the specific context of TE versus ICM cell fate
328 specification/segregation, prior to blastocyst formation. Indeed, such conclusions are supported by a lack of overt
329 apical polarity (PARD6B) defects or ectopic nuclear exclusion of YAP (as the transcriptional co-activator and Hippo-
330 pathway effector protein (Nishioka et al., 2009)) in outer-residing *Wwc2* knockdown blastomeres, by the 32-cell
331 (E3.5) stage (Fig. S7). However, normal YAP nuclear exclusion in inner-residing *Wwc2* knockdown cells was found
332 to be consistently less robust than that observed in equivalent inner-cells of control siRNA microinjected embryos,
333 possibly suggesting moderately impaired Hippo-signalling activation/ cytoplasmic YAP sequestration caused by
334 *Wwc2* knockdown (Fig. S7); although the observed nuclear YAP levels were far from equivalent to those observed
335 in outer residing blastomeres of the same embryos (Fig. S7). Such data are indicative of a potentially mild inhibition
336 of active Hippo-signalling in such inner *Wwc2* knockdown cells, by the 32-cell (E3.5) stage.

337 We next extended the analyses to the late blastocyst (E4.5) stage, assaying TE and EPI lineage markers (*i.e.*
338 CDX2 & NANOG) or PrE and EPI markers (*i.e.* GATA4 & NANOG or GATA4 & SOX2) as pairwise combinations
339 (Figs. 7 & S8). We again observed *Wwc2* knockdown clone specific cell number deficits (relayed into reduced total
340 blastocyst cell number) and nuclear morphology/cell division related phenotypes. Despite such defects, and
341 contrasting with the early blastocyst stage, the ratio of total outer (TE) to inner (ICM) cells was not significantly
342 different between *Wwc2* or control siRNA microinjection groups (across all assayed lineage combinations; Fig. 7d-
343 f); indicating a degree of regulative development during blastocyst maturation. However, collectively we noted
344 incidences of fragmented nuclei, indicative of apoptotic cell death, that were significantly more prevalent within the
345 ICM of *Wwc2* siRNA, versus control siRNA, microinjected embryo groups. Moreover, the observed apoptosis was
346 significantly enriched within the microinjected clone of *Wwc2* knockdown embryos, suggesting such ICM residing
347 cell clones are prone to an increased probability of cell death (Fig. 7b). Consistently, the overall and significantly
348 reduced contributions of *Wwc2* siRNA derived clones were more pronounced for ICM versus outer-cell populations
349 (Fig. S8). Focussing, on CDX2 and NANOG immuno-stained groups, we again noted a population of CDX2 negative
350 outer-cells and generally reduced CDX2 expression within the *Wwc2* knockdown clone (Fig. 7c). Moreover, the
351 significantly reduced number of ICM cells derived from the *Wwc2* knockdown clone did not segregate between

352 NANOG positive (indicative of EPI) and NANOG negative (potentially PrE) cells, as per marked control siRNA
353 clones (*i.e.* according to a clone's overall percentage contribution within the ICM), but were significantly biased to
354 populate the potential, NANOG negative, PrE (Fig. 7d). Considering all assayed embryos in the whole, the overall
355 reduction in size of the potential PrE (NANOG negative) population that was associated with clonal *Wwc2*
356 knockdown, was much less than that observed in the EPI (Fig. S8). This suggests inner *Wwc2* siRNA microinjection
357 derived clones are impaired in their contribution to sustain EPI numbers, by the late blastocyst (E4.5) stage, but are
358 able to differentiate to form PrE. This interpretation was supported by data directly assaying the two ICM lineages
359 (*i.e.* GATA4 in combination with either NANOG or SOX2; Figs. 7e & f, plus Fig. S8), whereby the characteristically
360 low number of inner *Wwc2* knockdown cells/clones observed, similarly segregated in a manner favouring the PrE
361 (marked by GATA4) over EPI (marked by either NANOG or SOX2); note, compensatory increases in EPI
362 contribution were also observed in the non-microinjected clone (Fig. S8). We also observed numerous examples of
363 fragmented/ apoptotic inner-cell nuclei displaying distinct immuno-reactivity for SOX2 (Fig.7c), suggesting the
364 increased incidence of apoptosis observed within the ICM residing and microinjected cell clones of *Wwc2*
365 knockdown embryos (Fig. 7b) is centred on specified EPI that is ultimately unable to be maintained (although it was
366 not possible to reliably quantify the number of SOX2 positive apoptotic nuclei). Interestingly, in *Wwc2* siRNA
367 microinjected embryo groups, we also observed a small population of marked ICM clones that expressed neither PrE
368 or EPI markers (comprising 4.6% of all ICM cells and 18.7% of the clone) that were not present in control siRNA
369 treated groups, potentially indicative of a further impairment in ICM cell fate derivation.
370 In conclusion, our late blastocyst cell fate analyses confirm *Wwc2* knockdown clone specific and autonomous
371 reductions in overall cell number, that more robustly affect the ICM versus TE. Such reductions are compensated for
372 by regulation within the non-injected clone, that ultimately preserves the overall TE:ICM ratio (albeit with fewer
373 overall cells). However, the lineage contribution of *Wwc2* knockdown clones within the ICM is biased against the
374 pluripotent EPI in favour of PrE differentiation, via an implicated mechanism possibly involving clone specific and
375 selective EPI apoptosis; suggesting a role for *Wwc2* in contributing to specified EPI maintenance that is additional
376 to that related to cell division, yet inherently difficult to experimentally resolve.
377
378 **Mouse embryo *Wwc2* siRNA knockdown phenotypes are revertible by recombinant/rescue HA-WWC2 protein**
379 **expression, associated with cell division generated mid-bodies.**
380 As with the described primary oocyte IVM experiments, we wanted to confirm that the uncovered mitotic
381 cell division phenotypes observed after *Wwc2* knockdown in embryos could also be rescued using the derived
382 recombinant siRNA-resistant *HA-Wwc2* mRNA construct. Thus, we repeated our marked clonal microinjection
383 experiments but included a third condition in which *Wwc2* siRNA was co-microinjected with *HA-Wwc2* mRNA.
384 Microinjected 2-cell (E1.5) stage embryos were then cultured until the early (E3.5) and late (E4.5) blastocyst stages
385 and total/clonal cell contributions to inner/outer-cell populations, plus the incidence of abnormal nuclear morphology,
386 calculated (Fig. 8). Compared with the control siRNA group, embryos microinjected with *Wwc2* siRNA alone
387 exhibited the typical clone autonomous phenotypes. However, under *Wwc2* siRNA conditions supplemented with co-
388 microinjected *HA-Wwc2* mRNA (the expression of which was confirmed, see below and Fig. 8d) the average number
389 and clonal/spatial composition of constituent early (E3.5) and late (E4.5) blastocyst cells was statistically
390 indistinguishable from control siRNA microinjections groups (with the only exception being a small reduction in the

391 ICM contribution of the non-microinjected clone by the late/E4.5 blastocyst stage; *i.e.* from 9.5±0.4 to 8.2±0.3).
392 Additionally, there was a complete rescue of the incidence of nuclei with abnormal morphology (with only one
393 exception in all blastomeres assayed – shown in Fig. 8d). Collectively, these data demonstrate the specificity of the
394 RNAi reagents (in both oocytes and embryos) used in this study and confirm *Wwc2* as a novel regulatory gene of cell
395 division dynamics and subsequent germane cell fate derivation.
396 As referenced above, the HA-epitope tag incorporated within the confirmed *HA-Wwc2* 'phenotypic rescue'
397 mRNA construct not only enabled us to verify its translation but also its sub-cellular localisation within the
398 microinjected clone, using an immuno-staining approach. Interestingly, given the clone autonomous cell
399 number/division defects observed after embryonic *Wwc2* knockdown, we consistently detected anti-HA immuno-
400 reactivity at structures typical of mitotic spindle derived mid-bodies (generated after cytokinesis), that were
401 particularly evident within the *HA-Wwc2* microinjected clones at the 32-cell stage (Fig. 8d & Fig. S9a). As a recent
402 study identified a critical role for uncharacteristically persistent interphase mid-bodies (referred to as 'interphase
403 microtubule bridges') as important MTOCs within the blastomeres of cleavage stage embryos (Zenker, White et al.,
404 2017), we assayed their number (immuno-staining for α-Tubulin and activated phospho-Aurora-B/pAURKB, as
405 recognised midbody markers – (Terada, Tatsuka et al., 1998)) in control and *Wwc2* knockdown embryos at the same
406 32-cell stage, but could not detect any statistically significant variation in their overall incidence (when corrected for
407 the reduced cell number caused by *Wwc2* knockdown - Fig. S9c-e). Hence, whilst *HA-Wwc2* derived recombinant
408 protein is consistently (in relation to *Wwc2* knockdown phenotypes) associated with cell division mid-bodies, the
409 removal of endogenous *Wwc2* mRNA does not appear to impair mid-body formation or persistence following
410 compromised cell divisions.
411

412 **DISCUSSION**

413

414 We have identified *Wwc2*, the sole murine WWC-domain containing paralog of the recognised Hippo-
415 pathway activator *Kibra* (Baumgartner et al., 2010, Genevet et al., 2010, Wennmann et al., 2014, Xiao et al., 2011a,
416 Yu et al., 2010), as a novel mitotic regulator of preimplantation mouse embryo cell cleavage divisions (Figs. 1-3)
417 and uncovered a conserved role during primary mouse oocyte meiotic maturation (Fig. 4), predicated on appropriate
418 activation/phosphorylation of the cell-cycle kinase AURKA (Figs. 5 and S6). Additionally, we have shown *Wwc2*
419 knockdown cell clones are compromised in ultimately contributing to the specified EPI lineage, by the late blastocyst
420 stage, being prone to apoptosis or disproportionate contribution to PrE (Figs. 7 and S8). Thus, these data implicate at
421 least two functional roles for *Wwc2* during early mouse development/reproduction; i) spatial and temporal regulation
422 of correct cell division spindle apparatus formation/function in both meiotic primary oocytes and early mitotic
423 embryonic blastomeres (each paradigms of typical and atypical, acentrosomal/acentriolar cell division, relative to
424 other mammalian species, respectively (Bennabi et al., 2016, Courtois et al., 2012, Gruss, 2018, Mogessie et al.,
425 2018, Namgoong & Kim, 2018, Severson et al., 2016)), and ii) affecting individual blastomere pluripotency and
426 differentiation potential, particularly with respect to EPI and PrE derivation in the ICM of late mouse blastocysts
427 (E4.5) (Figs. 7 and S8). However, the full extent of such a cell fate related role, is very difficult to experimentally
428 dissect, given the described cell division defects evident as early as the 8-cell (E2.5) stage after *Wwc2* knockdown.

429 Relating to cell fate regulation, the attainment of naïve pluripotency within specified EPI cells of the late
430 (E4.5) mouse blastocyst has recently been shown to be regulated via a heterogeneous mechanism of activated
431 TEAD1-mediated transcription (caused by YAP relocalisation from the cytoplasm to the nucleus), that promotes
432 ICM cell/EPI progenitor competition and elimination (by apoptosis) (Hashimoto & Sasaki, 2019). This contrasts with
433 earlier specification and segregation of outer TE from founder ICM populations, prior to the blastocyst stage, whereby
434 activated Hippo-signalling and YAP nuclear exclusion is required for inner-cells to actively retain pluripotency (*e.g.*
435 express *Sox2*) and resist TE differentiation (Sasaki, 2017). Hence, active Hippo-signalling seems to both support
436 initial pluripotency in ICM founders (*i.e.* confirmed - see (Sasaki, 2017)) but presumably needs to be suppressed in
437 EPI progenitors to promote naïve pluripotency (*i.e.* to permit nuclear YAP translocation, inferred from the literature
438 (Hashimoto & Sasaki, 2019)). Our data, although compounded by the additional cell division phenotypes, suggests
439 *Wwc2* (as a paralog of the Hippo-activator *Kibra*) may also contribute to germane Hippo-signalling regulation. For
440 example, relating to late blastocyst (E4.5) stage EPI specification, we find ICM-residing *Wwc2* knockdown clones,
441 although fewer than their non-microinjected clone counterparts, do not display the same equal contribution to
442 populate the EPI (NANOG+/SOX2+) and PrE (GATA4+) as observed in the non-specific siRNA microinjected
443 clones of control embryos (Figs. 7 and S8). Indeed, such clones statistically favour PrE over EPI contribution,
444 indicative of compromised pluripotent potential. Whether this is due to compromised Hippo-signalling activation
445 after initial internalisation prior to blastocyst formation, and/or relates to relative fitness deficiencies affecting their
446 ability to successfully compete to colonise specified EPI, is uncertain. However, an increased apoptotic ICM cell
447 number within *Wwc2* knockdown clones, often marked by detectable SOX2 protein expression (but never GATA4
448 immunofluorescence), observed in late (E4.5) blastocysts (Fig. 7b & c) is consistent with their competitive
449 elimination. Although, the possibility remains the apparent lack of EPI fitness, associated with *Wwc2* knockdown, is
450 caused by an initial pluripotency deficit in ICM founders. Nevertheless, our analysis of early stage (E3.5) clonal

451 *Wwc2* knockdown blastocysts, suggests the establishment of required differential Hippo-signalling between TE (*i.e.*
452 suppression) and ICM (*i.e.* activation) was largely intact (Figs. 6 and S7; *i.e.* CDX2, PARD6B, CDH1 and YAP
453 immuno-fluorescent staining). Although, the comparatively reduced (or sometimes absent) expression of outer-cell
454 CDX2 protein, plus less efficient YAP protein nuclear exclusion in inner-cells, in *Wwc2* knockdown clones
455 (compared with sister non-microinjected clones within the same embryo or non-specific siRNA microinjected clones
456 in control embryos; Figs. 6 and S7) implies some degree of mild early onset Hippo-signalling defect; potentially
457 becoming more manifest/relevant during blastocyst maturation/EPI specification. The EPI specific exclusion of
458 *Wwc2* knockdown clones may also be related increased levels of aneuploidy caused by the defective cell division
459 phenotypes. Indeed, it is known that experimentally derived clonal aneuploidy in preimplantation stage mouse
460 chimeras, is selectively eliminated from the EPI by apoptosis but tolerated within the extra-embryonic blastocyst
461 tissues (Bolton, Graham et al., 2016). The relatively mild early cell fate effects may also reflect functional redundancy
462 between WWC2 and KIBRA, whereby potential major Hippo-signalling defects caused by specific *Wwc2*
463 knockdown are compensated by continued and sufficient expression of *Kibra*; indeed, we demonstrated robust *Wwc2*
464 knockdown does not affect *Kibra* mRNA levels (Fig. 1 and S1). Support for functional redundancy between WWC-
465 domain proteins paralogs has been demonstrated in human cells (relating to KIBRA, WWC2 and WWC3
466 (Wennmann et al., 2014)) and genetic ablation of the mouse *Kibra* gene is developmentally viable (with adult mice
467 only exhibiting learning and memory deficits (Makuch, Volk et al., 2011)). Interestingly, our initial clonal dsRNA
468 mediated knockdown of *Kibra* and *Wwc2* expression, either in isolation or combination (Fig.1), demonstrated robust
469 down-regulation of *Kibra* alone did not impair formation of cavitated late (E4.5) blastocysts (comprising equal cell
470 numbers to control dsRNA groups), suggesting loss of the *Kibra* paralog could be tolerated, potentially due to
471 continued *Wwc2* expression. However, sole *Wwc2* knockdown caused the profound defects present in this study,
472 despite continued expression of *Kibra,* and were not exacerbated by co-down regulation of *Kibra*. Hence, if KIBRA
473 and WWC2 proteins share functional redundancy during mouse preimplantation development, it is likely only in
474 relation to Hippo-signalling regulation and not applicable to the described cell division roles of WWC2.
475 As described, siRNA mediated *Wwc2* knockdown causes cell autonomous deficits in total preimplantation
476 mouse embryo cell number (particularly affecting inner-cell populations), by the 16-cell (E3.0) stage (Figs. 2, 3 and
477 S2). Why reduced embryo cell numbers are manifest comparatively late, given initial microinjection is performed 2-
478 cell (E1.5) stage embryos is unclear. Possibly, all subsequent cell-cycles in *Wwc2* knockdown clones are elongated
479 in a manner that is only revealed on the whole embryo level by the 16-cell (E3.0) stage, implicating *Wwc2* as a
480 regulator of the atypically long cell-cycles of preimplantation mouse/mammalian embryo blastomeres (reviewed
481 (O'Farrell, Stumpff et al., 2004)). Alternatively, it may reflect the developmental point maternally provided WWC2
482 protein, unaffected by siRNA, is functionally depleted. However, it impossible here to directly probe WWC2 protein
483 expression, due to a lack of available antibodies. Although, we did confirm the abundant presence of poly-adenylated
484 maternal *Wwc2* mRNAs in both primary (associated with translating polysomes) and secondary mouse oocytes and
485 zygotes (Fig. 4a & b), that coupled with the functional role in meiotic maturation (Figs. 4, 5, S3 and S6), strongly
486 suggest maternal WWC2 protein inheritance in early cleavage stage embryos. The appearance of cell number deficits
487 from the 16-cell (E3.0) stage also temporally coincides with the first spatial segregation of blastomeres (*i.e.* outer-
488 and inner- positions), polarity/position dependant differential Hippo-signalling establishment and TE versus ICM
489 cell fate derivation (Sasaki, 2017). As *Wwc2* is a paralog of the confirmed Hippo-activator *Kibra* (Baumgartner et

490 al., 2010, Genevet et al., 2010, Wennmann et al., 2014, Xiao et al., 2011a, Yu et al., 2010), it is tempting to speculate
491 the developmental timing of the cell number phenotype is particularly relevant. However, our experimental data
492 suggest Hippo-signalling at this time (*i.e.* prior to blastocyst formation) is at most mildly affected by *Wwc2*
493 knockdown. Additionally, the onset of individual nuclear morphological phenotypes, indicative of defective cell
494 division/cytokinesis (*e.g.* mid-body association, bi-/multi-/micro-nucleation; Fig. 3), were already evident by the 8-
495 cell (E2.5) stage. Moreover, whilst average cell number was impaired in *Wwc2* knockdown embryos after the 8-cell
496 (E2.5) stage, it did not significantly increase again until the mid-blastocyst (E4.0) stage (remaining around 8-10 cells
497 after global *Wwc2* knockdown, through the 16-/32-cell, E3.0/E3.5, stage equivalents; Fig. 2). This is significant as
498 the mid-blastocyst (E4.0) stage reflects the developmental point at which the atypically acentrosomal/acentriolar cell
499 cleavage divisions of mouse embryos, in comparison with most other mammalian species, revert back to centrosomal
500 control, after *de novo* centrosome synthesis (Courtois et al., 2012) (although it could also reflect the waning effect of
501 *Wwc2* specific siRNA). Therefore, we propose our data demonstrate a role for WWC2 in regulating acentrosomal
502 cell division in preimplantation stage mouse blastomeres, prior to the mid-blastocyst (E4.0) stage. Moreover, that
503 WWC2 is a regulator of mitotic spindle formation/functional dynamics, as reflected in phenotypic nuclear
504 morphologies observed after *Wwc2* knockdown (Fig. 3). Supporting this hypothesis, we readily detected recombinant
505 HA-WWC2 protein (derived from microinjected siRNA resistant recombinant *HA-Wwc2* mRNA, used to
506 successfully elicit phenotypic rescue of *Wwc2* knockdown phenotypes – Figs. 8 and S5) in confirmed mitotic mid-
507 bodies up until the early blastocyst (E3.5) stage but much less easily by the late blastocyst (E4.5) stage (Figs. 8 and
508 S9); *i.e.* subsequent to *de novo* centrosome synthesis (Courtois et al., 2012). The hypothesis is further substantiated
509 by our data relating to primary oocyte maturation, in which GV stage oocytes depleted of *Wwc2* transcripts are
510 unable, again in the absence of centrosomes (Bennabi et al., 2016, Gruss, 2018, Mogessie et al., 2018, Namgoong &
511 Kim, 2018, Severson et al., 2016), to complete meiosis I and present with multiple spindle defects associated with
512 failed activation/phosphorylation of the key cell-cycle kinase, AURKA (Figs. 4, 5, S3 and S6). The importance of
513 AURK activity during early mouse embryo cell cleavage has been reported, whereby clonal siRNA mediated
514 downregulation of *Aurkb* and *Aurkc* expression respectively increases or decreases the rate of mitotic cell division
515 (*Aurkb* and *Aurkc* over-expression exhibit the opposing effects). Indeed, the reported cell number deficits associated
516 with *Aurkc* down regulation, strongly resemble those related to *Wwc2* knockdown. Increased *AurkC* expression was
517 also shown to potentiate pluripotent gene expression, whilst enhanced *Aurkb* expression impaired nuclear retention
518 of recombinant photo-activatable-OCT4 reporter protein (Li et al., 2017). It will be interesting to functionally probe
519 any potential link between WWC2 and AURKB/AURKC, in the context of potentially regulating pluripotency and
520 Hippo-pathway regulation, in future studies.

521 The first report to implicate WWC-domain containing proteins in mammalian Hippo-signalling,
522 demonstrated human KIBRA (in HEK293T cells) binding to, and stimulating the phosphorylation/activation, of
523 LATS1/2, leading to subsequent phosphorylation of YAP (Xiao et al., 2011a). The same authors later described
524 mitosis specific KIBRA phosphorylation catalysed by AURKA and/or AURKB at a highly conserved AURK
525 consensus/target motif (centred on Ser539), and showed that over-expression of a KIBRA mutant (S539A) promotes
526 precocious M-phase exit in a model of SAC arrest, despite continued activation of cyclin dependent kinase, CDK1
527 (Xiao, Chen et al., 2011b). Thus, implicating KIBRA as an important molecular component of M-phase
528 progression/dynamics. Indeed, the same group also demonstrated the requirement of KIBRA to fully

529 activate/phosphorylate AURKA, that in turn is responsible for LATS2 phosphorylation/activation, ensuring its
530 appropriate centrosomal localisation. Moreover, that siRNA mediated *KIBRA* transcript knockdown causes profound
531 spindle defects, lagging chromosomes and micronuclei formation, reminiscent of the uncovered *Wwc2* knockdown-
532 related phenotypes, plus centrosomal fragmentation in human MCF7 and HeLa cell line models (Zhang, Iyer et al.,
533 2012) (phenotypes typical of direct LATS2 disruption and known to promote centrosomal structural integrity
534 (Yabuta, Okada et al., 2007) and accumulation of gamma-tubulin required for initiating mitotic spindle assembly
535 (Abe, Ohsugi et al., 2006)). Interestingly, we have now confirmed the presence of the same AURK consensus motifs
536 in both murine KIBRA and WWC2 proteins (Fig. S10). It is therefore tempting to speculate the *Wwc2* knockdown
537 phenotypes we observe in preimplantation stage mouse embryos may be mechanistically related to those previously
538 described for human KIBRA, although with the caveat they function on the level of MTOC regulation, in the absence
539 of centrosomes/centrioles (Courtois et al., 2012) (for example, targeted genetic ablations of the *Lats1* and *Lats2* genes
540 in mice are not described in association with the preimplantation embryo cell division/cell number deficits typical of
541 *Wwc2* knockdown, nor those phenotypes described above in relation to other models of mitosis, rather, and only
542 present in early blastocysts as ectopic nuclear YAP localisations within ICM cells (Nishioka et al., 2009)). Therefore,
543 not all insights will be directly transferable. However, despite the lack of centrosomes in pre-mid-blastocyst stage
544 mouse embryos, classical key centrosome regulators are expressed and been shown to have functional cell division
545 roles. For example, genetic knockout of the M-phase cell-cycle regulator, Polo-like kinase 1 (*Plk1*), known to
546 cooperate with AURKA within centrosomes to mediated bi-polar spindle formation (Asteriti, De Mattia et al., 2015),
547 interestingly arrests at the same 8-cell (E2.5) developmental stage at which embryos subject to global *Wwc2*
548 knockdown first present with cell division defects (Figs. 2 and 3) (Lu, Wood et al., 2008). Moreover, a critical role
549 for the related *Plk4* gene, itself recognised as a key regulator of centriole formation/duplication (Bettencourt-Dias,
550 Rodrigues-Martins et al., 2005, Habedanck, Stierhof et al., 2005), has been demonstrated during acentrosomal mouse
551 blastomere division. Accordingly, active PLK4 protein localises within the coalescing MTOCs forming around
552 condensed chromatin and in cooperation with the centrosomal protein CEP152, promotes microtubule nucleation and
553 bi-polar spindle formation and experimental depletion of active PLK4 results in the formation of mono-polar
554 microtubule asters (Coelho et al., 2013). Hence, it will be interesting to further investigate the identified role of *Wwc2*
555 during early embryo acentrosomal cell division, through the prism of such pre-existing characterised, and MTOC-
556 related/regulating, molecular components. Furthermore, to test applicability of such potentially identified
557 mechanisms within the conceptually similar paradigm of acentrosomal meiotic divisions of the maturing primary
558 oocyte (also identified here as under control of *Wwc2*). Indeed, a role for PLK4 in mediating acentriolar spindle
559 assembly in mouse oocytes, was recently described, whereby MTOC resident PLK4 in cooperation with AURKA
560 participates in initiating microtubule nucleation around condensing chromosomal bivalents upon meiosis re-entry.
561 However, unlike in mitotic blastomeres, functional inhibition of PLK4 does not completely block bi-polar spindle
562 formation but rather extends assembly completion time. Moreover, the oocyte MTOC related roles of PLK4 and
563 AURKA are only partially overlapping, with AURKA contribution appearing to be dominant (*e.g.* catalytically
564 targeting the microtubule minus end stabiliser TACC3) (Bury et al., 2017) and distinct from the co-existing
565 mechanism of chromosome derived RAN-GTP gradient driven microtubule stabilisation in oocytes (as reviewed
566 (Bennabi et al., 2016, Gruss, 2018, Mogessie et al., 2018, Namgoong & Kim, 2018, Severson et al., 2016)). Clearly,
567 in the context of the *Wwc2* knockdown oocyte maturation phenotypes described here (that include failed AURKA

568 phosphorylation/activation), potential links between described PLK4/AURKA phenotypes and WWC2 merit further
569 investigation. They are also consistent with reports implicating AURKA in the regulation of MTOC dynamics and
570 microtubule spindle nucleation (Nguyen et al., 2018, Nguyen & Schindler, 2017, Solc et al., 2012, Swain et al., 2008).
571 However, importantly the described functional inhibition of PLK4 was shown to be associated with eventual polar
572 body formation (Bury et al., 2017), unlike after *Wwc2* knockdown (even after an extended IVM incubation time –
573 Fig. S3), indicating that whilst meiotic spindle assembly is affected/impaired by *Wwc2* knockdown (illustrated by a
574 25.7% incidence of complete spindle formation failure and a further 22.9% of oocytes exhibiting defective spindles
575 - Fig. 4e), other impediments to successful meiotic maturation must exist (potentially relating, although not
576 necessarily limited, to spindle migration, SAC, cytokines *etc.*). The comparative spread of observed meiotic
577 maturation failure phenotypes associated with *Wwc2* knockdown (*i.e.* failed spindle formation, defective spindles or
578 persistent/ non-dividing MI spindles – Fig. 4e) also suggests a degree of functional redundancy may exist in response
579 to loss of WWC2 protein; for example, potentially related to the compensatory abilities of three expressed AURK
580 paralogs (*i.e. Aurka*, *Aurkb* and *Aurkc*), as demonstrated in combinatorial genetic ablations in mouse oocytes (Nguyen
581 et al., 2018).
582 In conclusion, we have identified the ill-characterised WWC-domain containing mouse gene *Wwc2* as an
583 important cell-cycle regulator in both preimplantation mouse embryo blastomeres and maturing primary oocytes;
584 both paradigms of acentrosomal cell division. Additionally, we have uncovered evidence for *Wwc2,* as a paralog of
585 the classically described Hippo-signalling activator *Kibra*, in participating in cell fate regulation in regard to
586 blastocyst ICM pluripotency. Despite the compounding nature of the two identified *Wwc2* knockdown phenotypes,
587 it will be of great interest to experimentally determine the key molecular interactions and further understand the novel
588 roles played by WWC2 protein, in both mouse preimplantation embryo cell fate and mitosis and maturing primary
589 oocyte meiosis.
590

591 **MATERIALS & METHODS**

592

593 Mouse/mouse embryo related experimental procedures were approved and licensed by the local ethics
594 committee of the Biology Centre (in České Budějovice) of the Czech Academy of Sciences and by the responsible
595 committee of the Czech Academy of Sciences at the national level, in accordance with Czech and European Union
596 law.

597

598 **Embryo and oocyte culture and microinjection.**

599 2-cell stage (E1.5) embryo collection, from super-ovulated and mated 10 week old F1 hybrid (C57Bl6 x
600 CBA/W) female mice, and *in vitro* culture in mineral oil covered drops (~20 μL/ ~15 embryos) of commercial KSOM
601 (EmbryoMax® KSOM without Phenol Red; Merck, MR-020P-5F), was conducted as previously described
602 (Mihajlovic et al., 2015). Germinal vesicle (GV) stage primary oocytes were mechanically recovered from mature
603 Graafian follicles of dissected ovaries of dams after PMSG (pregnant mare serum gonadotrophin) hormone
604 stimulation (7.5U intraperitoneal injection of F1 hybrid strain, 48 hours prior). Recovered oocytes were placed into
605 pre-warmed (37°C) drops (~20 μl/ ~15 oocytes) of commercial CZB media (EmbryoMax® CZB media with Phenol
606 Red; Merck, MR-019-D) containing 100 μM IBMX (3-isobutyl-1-methylxanthine, a cAMP/cGMP
607 phosphodiesterase inhibitor that maintains GV meiosis I arrest), overlaid with mineral oil and incubated (37°C/ 5%
608 CO_2) for 2 hours prior to microinjection.

609 Individual blastomere dsRNA, siRNA or recombinant mRNA microinjections (or combinations thereof), plus
610 post-microinjection culture protocols, were performed on 2-cell stage embryos (in either one or both blastomeres)
611 according to defined protocols (Zernicka-Goetz, Pines et al., 1996), using apparatus formerly described (Mihajlovic
612 et al., 2015). Recovered GV staged oocytes were microinjected using a minimally adapted protocol; namely oocytes
613 were microinjected on 37°C heated stage in concaved glass microscope slides filled with CZB media (+ IBMX
614 inhibitor, 100 μM), overlaid with mineral oil. Post-microinjection, GV oocytes were returned to the incubator for
615 another 18 hours (to permit microinjected siRNA mediated gene knockdown or mRNA expression; CZB +IBMX
616 media) then transferred to fresh/pre-equilibrated CZB media drops lacking IBMX, to induce resumption of meiosis
617 I and *in vitro* maturation. Cultured (and microinjected) embryos and oocytes were assayed at various developmental
618 points, as dictated by individual experiments. As indicated, rhodamine-conjugated dextran beads (RDBs; 1 μg/ μl –
619 ThermoFisher Scientific, D1818) were co-microinjected to confirm successful blastomere/oocyte microinjection; a
620 summary of the origin and concentrations of all microinjected RNA species is given in supplementary methods tables
621 SM1. Non-microinjected embryos, or oocytes, (2-3 per microinjection experiment, per plate) served as culture
622 sentinels to confirm successful *in vitro* embryo development/oocyte maturation. In cases of AURKA chemical
623 inhibition (to confirm specifity of anti-p-AURKA antisera – Fig. S4), recovered GV oocytes were transferred from
624 IMBX containing CZB media to pre-equilibrated CZB media drops lacking IBMX but containing the specific
625 AURKA inhibitor, MLN8237 (1μM; Selleckchem, S1133).

626

627 **dsRNA and recombinant mRNA synthesis.**

628 Specific long dsRNA molecules targeting coding regions of mouse *Kibra* and *Wwc2* derived transcripts
629 (plus negative control GFP) were designed (and *in silico* validated using online E-RNAi resource (Horn & Boutros,

530 2010)) and synthesised. Briefly, gene specific PCR primer pairs, incorporating 5'- T7-derived RNA polymerase
531 promoters and spanning designed dsRNA complementary sequence, were used to derive *in vitro* transcription (IVM)
532 template, using mouse blastocyst (E3.5) cDNA as a template (or plasmid DNA for GFP). After agarose gel
533 verification, the double stranded DNA templates were used in preparatory IVM reactions, incorporating DNaseI and
534 single-stranded RNase treatment (MEGAscript T7; ThermoFisher Scientific, AMB13345), to generate dsRNA. The
535 integrity of derived *Kibra*-, *Wwc2*- and *GFP*-dsRNAs was confirmed by non-denaturing gel electrophoresis and
536 quantified (Nanodrop). The PCR primer sequences used are provided in supplementary methods table SM2.
537 Microinjected mRNA constructs were derived using commercially available IVT reaction kit (mMACHINE
538 T3; ThermoFisher Scientific, AM1348), in which restriction enzyme linearized (using *SfiI*) plasmid DNA was used
539 as template (2 µg) as follows; i. C-terminal GFP-fusion *Gap43* mRNA plasma membrane marker, from pRN3P-C-
540 term-GFP-Gap43 (Morris, Teo et al., 2010)), ii. C-terminal RFP-fusion histone H2B mRNA (from pRN3-C-term-
541 RFP-Hist1h2bb, derived in this study) and iii. siRNA-resistant N-terminal HA-tagged *Wwc2* mRNA (from pRN3P-
542 N-term-HA-siRNAres-Wwc2, derived here). All synthesised mRNAs were subject to post-synthesis 3' poly-
543 adenylation tailing (Poly(A) Tailing Kit - ThermoFisher Scientific, AM1350), confirmed by denaturing gel
544 electrophoresis and quantified (Nanodrop).
545
546 **Recombinant plasmid construct generation.**
547 Four recombinant plasmids (required for IVT) were generated, using standard molecular biological
548 protocols. RFP-histone H2B fusion protein (pRN3-C-term-RFP-Hist1h2bb) were derived by in frame cloning of a
549 high-fidelity PCR amplified cDNA (using Phusion® DNA polymerase, New England BioLabs, M05305) encoding
550 histone H2B (*Hist1h2bb,* lacking endogenous start and stop codons), flanked by oligonucleotide introduced
551 restriction sites (*NheI*), into the RNA transcription cassette plasmid pRN3-insert-RFP variant (vector encodes
552 required start and stop codons). Thus, generating required H2B-RFP fusion reporter, downstream of vector encoded
553 T3 RNA polymerase promoter (for IVT) and flanked by UTRs from the frog β-globin gene (Lemaire, Garrett et al.,
554 1995). The IVT plasmid encoding the siRNA-resistant N-terminal HA-tagged *Wwc2* mRNA (pRN3P-N-term-HA-
555 siRNAres-Wwc2) was created from an annotated full-length Riken mouse *Wwc2* cDNA clone (clone ID:
556 M5C1098O04, Source Bioscience) by deriving a high fidelity PCR product, with oligo introduced 5' (*SpeI*) and 3'
557 (*NotI*) restriction sites and an in frame N-terminal HA-epitope tag, and 'TA cloned' (after addition of 3' adenine
558 nucleotide overhangs) it into pGEM®-T-Easy plasmid vector (Promega, A1360). The derived plasmid was site
559 mutagenesised (commercial service; EuroFins) to alter the nucleotide (but not amino acid codon) sequence of the
560 siRNA (utilised in this study) recognition motif; details in supplementary figure S5. The recombinant gene sequence
561 was sub-cloned, using introduced *SpeI* and *NotI* restriction sites, into the multiple cloning site of the RNA
562 transcription cassette plasmid pRN3P (Zernicka-Goetz et al., 1996) to derive IVT competent pRN3P-N-term-HA-
563 siRNAres-Wwc2. All four derived plasmids were sequence verified and the PCR primers (or relevant details) used
564 to generate the required inserts are described in supplementary methods table SM3.
565
566 **Q-RT-PCR**
567 Per experimental condition, total RNA was extracted from ~30 (microinjected) mouse embryos (oocytes) *in*
568 *vitro* cultured to the desired developmental stage, using PicoPure RNA isolation kit (Arcturus Biosciences/

569 ThermoFisher Scientific, KIT0204), as instructed. Eluted RNA (10 µL) was DNaseI treated (DNA-*free* kit;
570 ThermoFisher Scientific, AM1906) and used to derive cDNA (30 µL), either via oligo-dT (embryos and oocyte) or
571 random hexamer (oocytes only) priming (Superscript-III Reverse Transcriptase; ThermoFisher Scientific,
572 18080085). 0.5 µl of diluted template cDNA (1:3, nuclease-free water) per real-time PCR reaction (10 µl – SYBR
573 Green PCR kit, Qiagen, 204143) was used to assay specific transcript abundance (CFX96 Real-Time System,
574 BioRad). *Kibra* and *Wwc2* transcript levels were internally normalised against those for *Tbp* (TATA-binding protein)
575 housekeeping gene and fold changes (±s.e.m.) derived using the ΔΔCt method (Livak & Schmittgen, 2001). A
576 minimum of two biological replicates of at least three technical replicates were employed; specific gene oligo primer
577 sequences (final reaction conc. 400 nM) are in supplementary methods table SM4.
578
579 **Immuno-fluorescent staining and confocal microscopy imaging**.
580 *In vitro* cultured (microinjected) embryos/oocytes were fixed (at required developmental stages) with 4%
581 para-formaldehyde, immuno-fluorescently stained and imaged in complete z-series by confocal microscopy (using
582 the FV10i confocal microscope, Olympus) as previously described (Mihajlovic et al., 2015); supplementary methods
583 table SM5 summarises the identity and combinations (plus employed concentrations) of primary and fluorescently
584 conjugated secondary antibodies used. Additionally, the majority of immuno-fluorescently stained embryos/oocytes
585 were counterstained for DNA, using DAPI containing mounting solution (Vectashield plus DAPI, Vector Labs) and
586 as indicated some embryo samples were also counterstained against filamentous-actin, using fluorescently-labelled
587 rhodamine-conjugated phalloidin (ThermoFisher, R415 - described in (Mihajlovic & Bruce, 2016)).
588
589 **Embryo/oocyte image analysis/ cell counting.**
590 The contribution of each individual cell, per fixed embryo sample (in control or *Kibra/Wwc2* gene RNAi
591 knock-down conditions), to either; inner (entirely encapsulated) outer (whereby a cell retains a cell contactless
592 domain) embryo compartments, emerging blastocyst cell lineages (defined by presence and/or absence of specific
593 and stated lineage marker protein expression), cell populations defined by the presence of a defining intra-cellular
594 feature (*e.g.* cell/nuclei morphological abnormalities, apoptosis or persistent mid-bodies) or presence within or
595 outwith a microinjected clone (distinguishable by a fluorescent injection marker signal, *i.e.* RDBs or recombinant
596 fluorescent fusion proteins) was determined by serial inspection of individual confocal micrograph z-sections of each
597 embryo, using commercial Fluoview ver.1.7.a (Olympus), Imaris (Bitplane) and freely available ImageJ software.
598 These calculated contributions were individually tabulated (see appropriate supplementary tables) and the mean of
599 cells within defined sub-populations, plus standard error of means (mean ± s.e.m.) determined. The statistical
700 significance between relevant experimental and control groups was determined using 2-tailed Student's t-tests
701 (experiment specific supplementary tables provide comprehensive summaries, plus all individual embryo derived
702 data). Relating to oocytes, a similar approach was used to assay the mean frequencies by which maturing oocytes
703 exhibit intra-cellular morphologies (revealed by combined immuno-fluorescent staining, *i.e.* α-TUBULIN and p-
704 AURKA and microinjected fluorescent reporter protein expression *i.e.* RFP-histone H2B) indicative of appropriate
705 or aberrant GV oocyte maturation (as categorised), at the indicated developmental time-point; similarly such data are
706 summarised in relevant supplementary tables, including individual oocyte derived data.
707

708 **Western blotting**

709 A precise number of oocytes per comparable experimental condition (~15-30) were washed in phosphate
710 buffer saline (PBS; Merck, P5493) containing polyvinyl alcohol (PVA; Merck, 341584), frozen in a residual volume
711 at -80°C, before lysis, in 10 µl of 10x SDS reducing agent/loading buffer (NuPAGE buffer, ThermoFisher Scientific,
712 NP 0004, ThermoFisher Scientific), by boiling at 100°C for 5 minutes. Loaded proteins were electrophoretically
713 separated on gradient precast 4–12% SDS–PAGE gels (ThermoFisher Scientific, NP0323) and transferred to
714 Immobilon P membranes (Merck group, IVPD00010) using a semi-dry blotting system (Biometra/ Analytik Jena)
715 for 25 minutes at 5 mA/ cm^{2}. Blotted membranes were blocked in 5% skimmed milk powder dissolved in 0.05%
716 Tween-Tris pH 7.4 buffered saline (TTBS) for 1 hour, briefly rinsed in TTBS and then incubated overnight at 4°C in
717 1% milk/TTBS containing primary antibody. Membranes were washed in three changes of TTBS buffer (20 minutes
718 each at room temperature) and horse-radish peroxidase conjugated secondary antibody added to the blot in 1%
719 milk/TTBS, for 1 hour (room temperature). Immuno-detected proteins were visualized by chemiluminescent
720 photographic film exposure (ECL kit; GE Life Sciences, RPN2232) and digitally scanned using a GS-800 calibrated
721 densitometer (Bio-Rad Laboratories). Antibody stripped membrane blots were re-probed, for loading controls, in an
722 identical manner. Supplementary methods tables SM6 details the utilised concentrations of the primary and
723 peroxidase-conjugated secondary antibodies used.
724

ACKNOWLEDGEMENTS

The authors acknowledge Marta Gajewska (Institute of Oncology, Warsaw, Poland) and Anna Piliszek (Institute of Genetics & Animal Breeding, Polish Academy of Sciences, Jastrzębiec, Poland) for providing the founder CBA/W mice used in this study, Martin Anger (Central European Institute of Technology (CEITEC)/ Veterinary Research Institute, Brno, Czech Republic) for valuable technical advice and discussions and Alena Krejčí (Faculty of Science, University of South Bohemia, České Budějovice, Czech Republic) for advice and pooling resources. The Animal Facility (Institute of Parasitology, Biology Centre of the Czech Academy of Sciences, České Budějovice, Czech Republic) is acknowledged for housing experimental mice. The research was supported by a Czech Science Foundation/ GA ČR grant (18-02891S) awarded to A.W.B. and a Grant Agency of the University of South Bohemia Ph.D. student award to G.V (GA JU: 015/2017/P).

AUTHOR CONTRIBUTION

A.W.B. & G.V. designed the experiments, participated in data analysis (plus A.Š.) and drafted the manuscript (plus A.Š.). G.V. performed all experiments and prepared samples for western blotting (performed by A.Š.). P.B. derived the recombinant DNA constructs and L.G. performed important ancillary experiments, ultimately not included in the final manuscript. A.W.B. coordinated the study. All authors approved the final version of the manuscript for publication.

CONFLICT OF INTERESTS

The authors declare that they have no conflict of interests.

749 **REFERENCES**

750

751 Abe Y, Ohsugi M, Haraguchi K, Fujimoto J, Yamamoto T (2006) LATS2-Ajuba complex regulates gamma-
752 tubulin recruitment to centrosomes and spindle organization during mitosis. FEBS Lett 580: 782-8
753 Alarcon VB (2010) Cell polarity regulator PARD6B is essential for trophectoderm formation in the
754 preimplantation mouse embryo. Biol Reprod 83: 347-58
755 Asteriti IA, De Mattia F, Guarguaglini G (2015) Cross-Talk between AURKA and Plk1 in Mitotic Entry and
756 Spindle Assembly. Front Oncol 5: 283
757 Baumgartner R, Poernbacher I, Buser N, Hafen E, Stocker H (2010) The WW domain protein Kibra acts
758 upstream of Hippo in Drosophila. Dev Cell 18: 309-16
759 Bennabi I, Terret ME, Verlhac MH (2016) Meiotic spindle assembly and chromosome segregation in
760 oocytes. J Cell Biol 215: 611-619
761 Bettencourt-Dias M, Rodrigues-Martins A, Carpenter L, Riparbelli M, Lehmann L, Gatt MK, Carmo N,
762 Balloux F, Callaini G, Glover DM (2005) SAK/PLK4 is required for centriole duplication and flagella
763 development. Curr Biol 15: 2199-207
764 Bolton H, Graham SJL, Van der Aa N, Kumar P, Theunis K, Fernandez Gallardo E, Voet T, Zernicka-
765 Goetz M (2016) Mouse model of chromosome mosaicism reveals lineage-specific depletion of aneuploid
766 cells and normal developmental potential. Nat Commun 7: 11165
767 Bury L, Coelho PA, Simeone A, Ferries S, Eyers CE, Eyers PA, Zernicka-Goetz M, Glover DM (2017) Plk4
768 and Aurora A cooperate in the initiation of acentriolar spindle assembly in mammalian oocytes. J Cell Biol
769 216: 3571-3590
770 Chazaud C, Yamanaka Y (2016) Lineage specification in the mouse preimplantation embryo.
771 Development 143: 1063-74
772 Cockburn K, Biechele S, Garner J, Rossant J (2013) The Hippo pathway member Nf2 is required for inner
773 cell mass specification. Curr Biol 23: 1195-201
774 Coelho PA, Bury L, Sharif B, Riparbelli MG, Fu J, Callaini G, Glover DM, Zernicka-Goetz M (2013) Spindle
775 formation in the mouse embryo requires Plk4 in the absence of centrioles. Dev Cell 27: 586-97
776 Courtois A, Schuh M, Ellenberg J, Hiiragi T (2012) The transition from meiotic to mitotic spindle assembly
777 is gradual during early mammalian development. J Cell Biol 198: 357-70
778 Davis JR, Tapon N (2019) Hippo signalling during development. Development 146
779 Frum T, Murphy TM, Ralston A (2018) HIPPO signaling resolves embryonic cell fate conflicts during
780 establishment of pluripotency in vivo. Elife 7
781 Frum T, Ralston A (2015) Cell signaling and transcription factors regulating cell fate during formation of
782 the mouse blastocyst. Trends Genet 31: 402-10
783 Frum T, Watts JL, Ralston A (2019) TEAD4, YAP1 and WWTR1 prevent the premature onset of
784 pluripotency prior to the 16-cell stage. Development 146
785 Genevet A, Wehr MC, Brain R, Thompson BJ, Tapon N (2010) Kibra is a regulator of the
786 Salvador/Warts/Hippo signaling network. Dev Cell 18: 300-8
787 Gruss OJ (2018) Animal Female Meiosis: The Challenges of Eliminating Centrosomes. Cells 7
788 Habedanck R, Stierhof YD, Wilkinson CJ, Nigg EA (2005) The Polo kinase Plk4 functions in centriole
789 duplication. Nat Cell Biol 7: 1140-6
790 Han Q, Kremerskothen J, Lin X, Zhang X, Rong X, Zhang D, Wang E (2018) WWC3 inhibits epithelial-
791 mesenchymal transition of lung cancer by activating Hippo-YAP signaling. Onco Targets Ther 11: 2581-
792 2591
793 Hashimoto M, Sasaki H (2019) Epiblast Formation by TEAD-YAP-Dependent Expression of Pluripotency
794 Factors and Competitive Elimination of Unspecified Cells. Dev Cell 50: 139-154 e5
795 Hassold T, Hunt P (2001) To err (meiotically) is human: the genesis of human aneuploidy. Nat Rev Genet
796 2: 280-91
797 Hirate Y, Hirahara S, Inoue K, Kiyonari H, Niwa H, Sasaki H (2015) Par-aPKC-dependent and -
798 independent mechanisms cooperatively control cell polarity, Hippo signaling, and cell positioning in 16-cell
799 stage mouse embryos. Dev Growth Differ 57: 544-56
800 Hirate Y, Hirahara S, Inoue K, Suzuki A, Alarcon VB, Akimoto K, Hirai T, Hara T, Adachi M, Chida K, Ohno
801 S, Marikawa Y, Nakao K, Shimono A, Sasaki H (2013) Polarity-dependent distribution of angiomotin
802 localizes Hippo signaling in preimplantation embryos. Curr Biol 23: 1181-94

803 Horn T, Boutros M (2010) E-RNAi: a web application for the multi-species design of RNAi reagents--2010
804 update. Nucleic Acids Res 38: W332-9
805 Johnson MH, Ziomek CA (1981) The foundation of two distinct cell lineages within the mouse morula. Cell
806 24: 71-80
807 Koncicka M, Tetkova A, Jansova D, Del Llano E, Gahurova L, Kracmarova J, Prokesova S, Masek T,
808 Pospisek M, Bruce AW, Kubelka M, Susor A (2018) Increased Expression of Maturation Promoting Factor
809 Components Speeds Up Meiosis in Oocytes from Aged Females. Int J Mol Sci 19
810 Kono K, Tamashiro DA, Alarcon VB (2014) Inhibition of RHO-ROCK signaling enhances ICM and
811 suppresses TE characteristics through activation of Hippo signaling in the mouse blastocyst. Dev Biol 394:
812 142-55
813 Kovarikova V, Burkus J, Rehak P, Brzakova A, Solc P, Baran V (2016) Aurora kinase A is essential for
814 correct chromosome segregation in mouse zygote. Zygote 24: 326-37
815 Lemaire P, Garrett N, Gurdon JB (1995) Expression cloning of Siamois, a Xenopus homeobox gene
816 expressed in dorsal-vegetal cells of blastulae and able to induce a complete secondary axis. Cell 81: 85-
817 94
818 Leung CY, Zernicka-Goetz M (2013) Angiomotin prevents pluripotent lineage differentiation in mouse
819 embryos via Hippo pathway-dependent and -independent mechanisms. Nat Commun 4: 2251
820 Li W, Wang P, Zhang B, Zhang J, Ming J, Xie W, Na J (2017) Differential regulation of H3S10
821 phosphorylation, mitosis progression and cell fate by Aurora Kinase B and C in mouse preimplantation
822 embryos. Protein Cell 8: 662-674
823 Livak KJ, Schmittgen TD (2001) Analysis of relative gene expression data using real-time quantitative PCR
824 and the 2(-Delta Delta C(T)) Method. Methods (San Diego, Calif 25: 402-8
825 Lu LY, Wood JL, Minter-Dykhouse K, Ye L, Saunders TL, Yu X, Chen J (2008) Polo-like kinase 1 is
826 essential for early embryonic development and tumor suppression. Mol Cell Biol 28: 6870-6
827 Makuch L, Volk L, Anggono V, Johnson RC, Yu Y, Duning K, Kremerskothen J, Xia J, Takamiya K, Huganir
828 RL (2011) Regulation of AMPA receptor function by the human memory-associated gene KIBRA. Neuron
829 71: 1022-9
830 Mihajlovic AI, Bruce AW (2016) Rho-associated protein kinase regulates subcellular localisation of
831 Angiomotin and Hippo-signalling during preimplantation mouse embryo development. Reprod Biomed
832 Online 33: 381-90
833 Mihajlovic AI, Bruce AW (2017) The first cell-fate decision of mouse preimplantation embryo development:
834 integrating cell position and polarity. Open Biol 7
835 Mihajlovic AI, FitzHarris G (2018) Segregating Chromosomes in the Mammalian Oocyte. Curr Biol 28:
836 R895-R907
837 Mihajlovic AI, Thamodaran V, Bruce AW (2015) The first two cell-fate decisions of preimplantation mouse
838 embryo development are not functionally independent. Sci Rep 5: 15034
839 Mogessie B, Scheffler K, Schuh M (2018) Assembly and Positioning of the Oocyte Meiotic Spindle. Annu
840 Rev Cell Dev Biol 34: 381-403
841 Morris SA, Teo RT, Li H, Robson P, Glover DM, Zernicka-Goetz M (2010) Origin and formation of the first
842 two distinct cell types of the inner cell mass in the mouse embryo. Proc Natl Acad Sci U S A 107: 6364-9
843 Nagaoka SI, Hassold TJ, Hunt PA (2012) Human aneuploidy: mechanisms and new insights into an age-
844 old problem. Nat Rev Genet 13: 493-504
845 Namgoong S, Kim NH (2018) Meiotic spindle formation in mammalian oocytes: implications for human
846 infertility. Biol Reprod 98: 153-161
847 Nguyen AL, Drutovic D, Vazquez BN, El Yakoubi W, Gentilello AS, Malumbres M, Solc P, Schindler K
848 (2018) Genetic Interactions between the Aurora Kinases Reveal New Requirements for AURKB and
849 AURKC during Oocyte Meiosis. Curr Biol 28: 3458-3468 e5
850 Nguyen AL, Schindler K (2017) Specialize and Divide (Twice): Functions of Three Aurora Kinase
851 Homologs in Mammalian Oocyte Meiotic Maturation. Trends Genet 33: 349-363
852 Nishioka N, Inoue K, Adachi K, Kiyonari H, Ota M, Ralston A, Yabuta N, Hirahara S, Stephenson RO,
853 Ogonuki N, Makita R, Kurihara H, Morin-Kensicki EM, Nojima H, Rossant J, Nakao K, Niwa H, Sasaki H
854 (2009) The Hippo signaling pathway components Lats and Yap pattern Tead4 activity to distinguish mouse
855 trophectoderm from inner cell mass. Dev Cell 16: 398-410
856 Nishioka N, Yamamoto S, Kiyonari H, Sato H, Sawada A, Ota M, Nakao K, Sasaki H (2008) Tead4 is
857 required for specification of trophectoderm in pre-implantation mouse embryos. Mechanisms of
858 development 125: 270-83

O'Farrell PH, Stumpff J, Su TT (2004) Embryonic cleavage cycles: how is a mouse like a fly? Curr Biol 14: R35-45
Rossant J (2016) Making the Mouse Blastocyst: Past, Present, and Future. Curr Top Dev Biol 117: 275-88
Rossant J (2018) Genetic Control of Early Cell Lineages in the Mammalian Embryo. Annu Rev Genet 52: 185-201
Salles FJ, Darrow AL, O'Connell ML, Strickland S (1992) Isolation of novel murine maternal mRNAs regulated by cytoplasmic polyadenylation. Genes Dev 6: 1202-12
Sanders JR, Jones KT (2018) Regulation of the meiotic divisions of mammalian oocytes and eggs. Biochem Soc Trans 46: 797-806
Sasaki H (2017) Roles and regulations of Hippo signaling during preimplantation mouse development. Dev Growth Differ 59: 12-20
Saskova A, Solc P, Baran V, Kubelka M, Schultz RM, Motlik J (2008) Aurora kinase A controls meiosis I progression in mouse oocytes. Cell Cycle 7: 2368-76
Sathananthan AH, Kola I, Osborne J, Trounson A, Ng SC, Bongso A, Ratnam SS (1991) Centrioles in the beginning of human development. Proc Natl Acad Sci U S A 88: 4806-10
Schatten H, Sun QY (2009) The role of centrosomes in mammalian fertilization and its significance for ICSI. Mol Hum Reprod 15: 531-8
Severson AF, von Dassow G, Bowerman B (2016) Oocyte Meiotic Spindle Assembly and Function. Curr Top Dev Biol 116: 65-98
Solc P, Baran V, Mayer A, Bohmova T, Panenkova-Havlova G, Saskova A, Schultz RM, Motlik J (2012) Aurora kinase A drives MTOC biogenesis but does not trigger resumption of meiosis in mouse oocytes matured in vivo. Biol Reprod 87: 85
Strumpf D, Mao CA, Yamanaka Y, Ralston A, Chawengsaksophak K, Beck F, Rossant J (2005) Cdx2 is required for correct cell fate specification and differentiation of trophectoderm in the mouse blastocyst. Development 132: 2093-102
Swain JE, Ding J, Wu J, Smith GD (2008) Regulation of spindle and chromatin dynamics during early and late stages of oocyte maturation by aurora kinases. Mol Hum Reprod 14: 291-9
Terada Y, Tatsuka M, Suzuki F, Yasuda Y, Fujita S, Otsu M (1998) AIM-1: a mammalian midbody-associated protein required for cytokinesis. EMBO J 17: 667-76
Wennmann DO, Schmitz J, Wehr MC, Krahn MP, Koschmal N, Gromnitza S, Schulze U, Weide T, Chekuri A, Skryabin BV, Gerke V, Pavenstadt H, Duning K, Kremerskothen J (2014) Evolutionary and molecular facts link the WWC protein family to Hippo signaling. Mol Biol Evol 31: 1710-23
White MD, Zenker J, Bissiere S, Plachta N (2018) Instructions for Assembling the Early Mammalian Embryo. Dev Cell 45: 667-679
Wicklow E, Blij S, Frum T, Hirate Y, Lang RA, Sasaki H, Ralston A (2014) HIPPO pathway members restrict SOX2 to the inner cell mass where it promotes ICM fates in the mouse blastocyst. PLoS Genet 10: e1004618
Xiao L, Chen Y, Ji M, Dong J (2011a) KIBRA regulates Hippo signaling activity via interactions with large tumor suppressor kinases. J Biol Chem 286: 7788-96
Xiao L, Chen Y, Ji M, Volle DJ, Lewis RE, Tsai MY, Dong J (2011b) KIBRA protein phosphorylation is regulated by mitotic kinase aurora and protein phosphatase 1. J Biol Chem 286: 36304-15
Yabuta N, Okada N, Ito A, Hosomi T, Nishihara S, Sasayama Y, Fujimori A, Okuzaki D, Zhao H, Ikawa M, Okabe M, Nojima H (2007) Lats2 is an essential mitotic regulator required for the coordination of cell division. J Biol Chem 282: 19259-71
Yagi R, Kohn MJ, Karavanova I, Kaneko KJ, Vullhorst D, DePamphilis ML, Buonanno A (2007) Transcription factor TEAD4 specifies the trophectoderm lineage at the beginning of mammalian development. Development 134: 3827-36
Yu J, Zheng Y, Dong J, Klusza S, Deng WM, Pan D (2010) Kibra functions as a tumor suppressor protein that regulates Hippo signaling in conjunction with Merlin and Expanded. Dev Cell 18: 288-99
Zenker J, White MD, Templin RM, Parton RG, Thorn-Seshold O, Bissiere S, Plachta N (2017) A microtubule-organizing center directing intracellular transport in the early mouse embryo. Science 357: 925-928
Zernicka-Goetz M, Pines J, Ryan K, Siemering KR, Haseloff J, Evans MJ, Gurdon JB (1996) An indelible lineage marker for Xenopus using a mutated green fluorescent protein. Development 122: 3719-24

914 Zhang L, Iyer J, Chowdhury A, Ji M, Xiao L, Yang S, Chen Y, Tsai MY, Dong J (2012) KIBRA regulates
915 aurora kinase activity and is required for precise chromosome alignment during mitosis. J Biol Chem 287:
916 34069-77
917 Zhang Y, Yan S, Chen J, Gan C, Chen D, Li Y, Wen J, Kremerskothen J, Chen S, Zhang J, Cao Y (2017)
918 WWC2 is an independent prognostic factor and prevents invasion via Hippo signalling in hepatocellular
919 carcinoma. J Cell Mol Med 21: 3718-3729

920 **FIGURE LEGENDS**

921

922 **Figure 1: dsRNA mediated WWC-domain containing gene (*Kibra* and *Wwc2*) expression knockdown in**
923 **preimplantation stage mouse embryos is associated (*Wwc2*) reduced cell number. a)** Experimental schema of
924 *Kibra* and *Wwc2* specific dsRNA (plus *EGFP n*egative control) embryo microinjection mediated global mRNA
925 knockdown, followed by *in vitro* culture to either 8-cell (E2.5) or 32-cell (E3.5) stage and Q-RT-PCR analysis (upper).
926 Normalised mRNA expression of either *Kibra* or *Wwc2* derived mRNAs after microinjection of stated dsRNA at the
927 stated developmental stage (lower; error bars represent s.e.m. and n=3). **b)** Experimental schema, similar to a),
928 describing clonal *Kibra*, *Wwc2* or *Kibra+Wwc2* knockdown (microinjection of one cell at the 2-cell/E1.5 stage) and
929 total cell number assay (via fixed embryo DAPI staining) at the late blastocyst, >64-cell (E4.5) stage (upper). Average
930 total cell numbers per embryo in each stated dsRNA microinjection group is shown (lower chart). **c)** Experimental
931 strategy to knockdown *Wwc2* expression (as in b) in a marked clone, by co-microinjection of *Wwc2* dsRNA with
932 rhodamine conjugated dextran microbeads (RDBs; fluorescent lineage marker) and assay clonal contribution at the
933 16-cell (E3.0) stage (upper). Average total cell number per clone (*i.e.* 'Inj'. vs. 'Non') in *Wwc2* or control dsRNA
934 microinjection groups are shown, as determined by the relative position of individual cells within the embryo (*i.e.*
935 encapsulated inside or with a cell contactless domain on the outside; lower chart). In panels b) & c) chart error bars
936 represent s.e.m. and 'n' numbers are indicated; statistically significant differences (2-tailed students t-test) between
937 the experimental microinjection groups (asterisks), or clones ('Inj.' vs. 'Non') within a group (double crosses), are
938 highlighted with statistical confidence intervals of $p<0.05$ and $p<0.005$, as denoted by one or two significance
939 markers, respectively; in panel b) a lack of significant difference between the compared groups is marked 'n.s.'.
940 Supplementary tables ST1 and ST2 summarise the statistical analysis and individual embryo data.

941

942 **Figure 2: siRNA mediated global *Wwc2* knockdown causes persistent preimplantation stage cell number**
943 **deficits from the 8-cell stage onwards: a)** Experimental design; non-specific control or *Wwc2*-specific siRNA were
944 co-microinjected with RDBs, into both blastomeres at the 2-cell (E1.5) stage, and *in vitro* cultured, fixed and subject
945 to total cell assay count (via DAPI and phalloidin staining) at the indicated developmental stage. A separate group of
946 microinjected embryos at the 32-cell stage were subject to normalised *Wwc2*-specific Q-RTPCR to assay knockdown
947 efficiency. **b)** Q-RTPCR data detailing the extent of endogenous *Wwc2* expression knockdown caused by
948 microinjected *Wwc2*-specific siRNA at the 32-cell (E3.5) stage (error bars denote s.e.m. of triplicate measurements,
949 n=3). **c)** Average total cell number in control (blue bars) or *Wwc2*-specific (green bars) siRNA microinjected embryos
950 at each indicated preimplantation developmental stages (the number of embryos in each assayed group is indicated).
951 Errors represent s.e.m. and 2-tailed student t-test derived statistical significance between the control and *Wwc2*
952 knockdown groups, at defined developmental stages, indicated (** $p<0.005$). Supplementary tables ST3-ST8
953 summarise the statistical analysis and individual embryo data in each experimental group. Note, additional data
954 describing the frequency of observable cell morphological/ division defects, obtained from this exact same dataset
955 are presented in Fig. 3.

956

957 **Figure 3: Global *Wwc2* knockdown mediated cell numbers deficits are coincident with accumulated cell**
958 **morpholoßgies consistent with defective cell division. a)** Schematic of experimental design whereby 2-cell (E1.5)

959 stage embryos microinjected with either control or *Wwc2*-specific siRNA were *in vitro* cultured to the indicated
960 developmental stage, fixed and assayed for total cell number (as described in Fig. 2) or the incidence of abnormal
961 cell/embryo morphology indicative of aberrant cell division, as determined by DAPI and rhodamine conjugated
962 phalloidin staining (note, data described in this figure are derived from same experiments as those described in Fig.
963 2). **b)** Exemplar confocal micrograph z-sections of *Wwc2*-specific siRNA microinjected embryos at the 32-cell (E3.5)
964 stage, illustrating three distinct categories of observed phenotypic morphological defects; i. abnormal nuclear
965 morphology (including chromatin mid body association - left), ii. cytokinesis defects defined by presence of two
966 nuclei per cell (centre), iii. presence of multiple (*i.e.* >3) nuclei and/or micronuclei per cell (right) and iv. a composite
967 of categorised defects highlighted by colour coded arrows in single embryo confocal z-section projection (green
968 boarder). DAPI (white) and cortical F-actin (red); scale bar = 20 μm. Yellow arrows highlight relevant defects and
969 the yellow asterisk shows an example of an individual nuclei of abnormal shape/ morphology. **c)** Frequencies of each
970 the observed categories of phenotypic/ morphological defect (*i.e.* micronuclei; blue, abnormal nuclei; yellow and
971 failed cytokinesis; green) or a combination of at least two or more (red) in control siRNA (left) and *Wwc2*-specific
972 siRNA (right) microinjected embryos, at the indicated developmental stage (numbers of embryos in each group is
973 highlighted); data demonstrate defect incidence per embryo (in at least one constituent blastomere – upper row of
974 charts) or on a per cell assayed basis (lower row of charts). Supplementary tables ST3-ST8 summarise the statistical
975 analysis and individual embryo data in each experimental group.
976
977 **Figure 4: *Wwc2* mRNA is required for mouse oocyte meiotic maturation. a)** Published microarray (Wang et al.,
978 2004, blue line) and generated Q-RT-PCR (bar charts) normalised *Wwc2* mRNA expression in germinal vesicle and
979 metaphase II arrested oocytes (GV and MII) and fertilised zygotes (Tbp normalised expression, relative to GV stage
980 expression). Note, microarray data derived from oligo-dT primed reverse transcription and Q-RT-PCR from both
981 oligo-dT (black bars) and random hexamer priming (red bars); error bars represent s.e.m. and n=3. **b)** Taken from
982 our published mRNA-Seq dataset of polysome-associated (red) and non-associated (blue) transcripts in *in vitro*
983 maturing mouse oocytes (after germinal vesicle breakdown/ GVBD +3 hours) (Koncicka *et al.,* 2018). **c)**
984 Experimental schema of *Wwc2* transcript knockdown in GV oocytes by microinjected *Wwc2* siRNA (plus control
985 siRNA and non-microinjected controls), 18 hour incubation in IMBX containing media (to prevent GVBD), 16 hour
986 *in vitro* oocyte maturation (IVM – minus IMBX treatment) and confocal microscopy/ Q-RT-PCR analysis; co-
987 microinjected RDBs were used as injection control marker. **d)** Q-RT-PCR data of normalised (against *Tbp* transcripts)
988 *Wwc2* mRNA levels in control and *Wwc2* siRNA microinjected GV oocytes matured to the MII stage; expressed as
989 percentage *Wwc2* mRNA knockdown, versus control (left), and normalised expression levels (right - error bars
990 represent s.e.m. and n=3). **e)** Charts (left) detailing successful maturation frequencies of control non-microinjected
991 (Non-Inj), microinjected control siRNA (Con. siRNA) and microinjected *Wwc2* siRNA GV oocytes, to the MII stage
992 or preceding phenotypic stages. Examples of successfully matured MII oocytes (note, extruded first polar body/PB1)
993 and the quantified categorised phenotypes are shown as confocal z-section micrographs (right – α-Tubulin in green
994 and DAPI DNA pseudo-coloured red; scale bar = 20 μm). Supplementary tables ST14 summarise the statistical
995 analysis and individual oocyte data used to generate the figure.
996

997 **Figure 5: *Wwc2* knockdown induced GV oocyte IVM phenotypes are associated with failed Aurora-A**
998 **(AURKA) phosphorylation/activation; both rescuable by co-microinjection of siRNA resistant *HA-Wwc2***
999 **mRNA. a)** Experimental schema of GV oocyte microinjection conditions; *i.e. Wwc2* siRNA or control siRNA alone
000 or *Wwc2* siRNA + *HA-Wwc2* (siRNA resistant) mRNA, each co-microinjected with either RDBs (for western blot
001 analysis) or RFP-H2B mRNA (IF – fluorescent marker). Microinjected (plus non-microinjected control) GV oocytes
002 were incubated in IMBX containing media (18 hours - to prevent GVBD), subject to IVM (max. 16 hours – media
003 minus IMBX) and processed for western blotting and IF at designated oocyte maturation time-points (assaying
004 phospho-Aurora/ p-AURKA levels) or assayed for developmental progression/*Wwc2* knockdown induced IVM
005 phenotypes. **b)** Western blots of activated p-AURKA levels (plus GAPDH housekeeping control), at indicated stages
006 of oocyte maturation (note, GV; +0 hours relative to IMBX washout, metaphase of meiosis I/ MI; +7 hours and MII;
007 +16 hours), in either control or *Wwc2* siRNA microinjected, or non-microinjected conditions. **c)** Exemplar single
008 confocal z-section IF micrographs of control (left) or *Wwc2* siRNA (right) IVM cultured microinjected oocytes to
009 the MII stage (relative to control; 16 hours post-IBMX) stained for p-AURKA (green) and α-TUBULIN (white) and
010 labelled with RFP-H2B chromatin reporter (red); insets show zoomed region of meiotic spindle. *Wwc2* siRNA
011 microinjection group example image is over-saturated compared to control (illustrating lack of spindle associated
012 pARUKA); PB1 (control siRNA) denotes the extruded first polar body and the scale bars represents 20 μm. **d)** Charts
013 detailing the maturation of control siRNA, *Wwc2* siRNA and *Wwc2* siRNA + *HA-Wwc2* mRNA GV oocytes at staged
014 time-points after IBMX removal; as described by the percentage of oocytes at any of the stated IVM stages or
015 categorised phenotypes (typically associated with *Wwc2* knockdown – see Fig. 7). **e)** Western blot of activated p-
016 AURKA levels (plus GAPDH housekeeping control), at the MII stage (16 hours post-IVM), in either control siRNA,
017 *Wwc2* siRNA or *Wwc2* siRNA + *HA-Wwc2* mRNA initially microinjected GV oocytes. Supplementary tables S16-
018 19 summarise the statistical analysis and individual oocyte data used to generate the figure.
019
020 **Figure 6: Outer trophectoderm (TE) versus ICM derivation in clonal *Wwc2* gene knockdown at the early**
021 **blastocyst stage. a)** Experimental strategy for *Wwc2* expression knockdown in a marked clone (representing 50% of
022 the embryo) by co-microinjection (in one blastomere of 2-cell/E1.5 stage embryos) of *Wwc2* siRNA and GAP43-
023 GFP mRNA (stable plasma membrane fluorescent lineage marker – 'Inj.') and an immunofluorescence (IF) based
024 assay of clonal contribution ('Inj' vs. 'Non') to CDX2 (TE marker) positive or negative cells, plus outer and inner-
025 cell embryo populations, at 32-cell (E3.5) stage (versus similar control siRNA microinjections). **b)** Exemplar confocal
026 z-section micrographs of IF stained blastocysts (individual greyscale channels plus merged image; CDX2 is red)
027 from control and *Wwc2* siRNA microinjected groups. Note, white arrows and the yellow arrow head denote DAPI
028 stained micronuclei and a bi-nucleated cell uniquely found within the *Wwc2* siRNA microinjected clone, respectively.
029 Similarly, blue and white asterisks denote respective low level (compared to non-injected clone) or undetectable
030 outer-cell CDX2 protein expression in *Wwc2* knockdown clones. The number of embryos in each group is provided;
031 scale bar equals 20μm. **c)** Left - pie charts detailing the average distribution of detectable CDX2 protein expression
032 between the control and *Wwc2* siRNA groups, in both outer or ICM cells (note, pie chart areas for each spatial
033 population are scaled to that summarising the whole embryo; similarly, the pie chart area describing the whole embryo
034 in the *Wwc2* siRNA condition is scaled to that in the control siRNA group). Right - average clonal contribution ('Inj'
035 vs. 'Non') of outer and ICM cells in control (blue bars) and *Wwc2* siRNA (green bars) microinjected embryos,

036 irrespective of CDX2 expression. **d)** As in c) only describing the clonal contribution of CDX2 expressing (or not)
037 cells to outer and ICM populations, as a fraction of the total sub-population size (left - pie charts) or in raw average
038 cell number (right – bar charts) In panel c) and d) charts, errors represent s.e.m. and 2-tailed student t-test derived
039 statistical significance between the control and *Wwc2* knockdown groups (asterisks), or clones ('Inj.' vs 'Non') within
040 a group (double crosses), are highlighted with statistical confidence intervals of $p<0.05$ and $p<0.005$, as denoted by
041 one or two significance markers, respectively. Supplementary tables ST20 summarise the statistical analysis and
042 individual embryo data.
043
044 **Figure 7: Overall cell lineage derivation in clonal *Wwc2* gene knockdown at the late blastocyst stage. a)**
045 Experimental strategy for *Wwc2* expression knockdown in a marked clone (representing 50% of the embryo) by co-
046 microinjection (in one blastomere of 2-cell/E1.5 stage embryos) of *Wwc2* siRNA and GAP43-GFP mRNA (stable
047 plasma membrane fluorescent lineage marker – 'Inj.') and an IF based assay of clonal contribution ('Inj' vs. 'Non')
048 to blastocyst protein lineage marker (TE; CDX2, PrE; GATA4, EPI; NANOG or SOX2; assayed in combination –
049 see below) expressing cells, plus outer and inner-cell embryo populations, at >64-cell, late blastocyst (E4.5) stage
050 (versus similar control siRNA microinjections). **b)** Average number of apoptotic cells observed in control and *Wwc2*
051 siRNA microinjected embryo groups (averaged across all IF regimes – see below) between outer and inner cell
052 populations and clones ('Inj.' vs. 'Non'); errors represent s.e.m. and 2-tailed student t-test derived statistical
053 significance between the control and *Wwc2* knockdown groups (asterisks), or clones ('Inj.' vs 'Non') within a group
054 (double crosses), are highlighted with statistical confidence intervals of $p<0.05$ and $p<0.005$, as denoted by one or
055 two significance markers, respectively. **c)** Exemplar confocal z-section micrographs of IF stained blastocysts
056 (individual greyscale channels plus merged image, in which assayed combinations of cell lineage markers are
057 respectively coloured green and red; CDX2 & NANOG, GATA4 & NANOG and GATA4 and SOX2) from control
058 and *Wwc2* siRNA microinjected groups. Within the *Wwc2* siRNA microinjected clone, yellow arrows denote
059 apoptotic cell remnants, blue arrows interphase ICM cells that neither express GATA4 or NANOG, the yellow arrow
060 head a bi-nucleated cell whereas blue or white asterisks highlight outer-cells with basal or undetectable CDX2
061 expression, respectively. The number of assayed embryos in each control ('Con') and *Wwc2* siRNA ('KD')
062 microinjection group is provided; scale bar equals 20µm. **d)** Pie charts detailing, in the left panel, the average
063 distribution of detectable CDX2 and NANOG protein expression between the control and *Wwc2* siRNA groups, in
064 both outer or ICM cells (note, pie chart areas for each spatial population are scaled to that summarising the whole
065 embryo; similarly the pie chart area describing the whole embryo in the *Wwc2* siRNA condition is scaled to that in
066 the control siRNA group). Central and right panels contain pie charts describing the clonal contribution of CDX2 and
067 NANOG expressing (or not) cells to outer and ICM populations, as a fraction of the total sub-population size. **e)** As
068 in d) only assaying NANOG (EPI) and GATA4 (PrE) expression. **f)** As in d) only assaying SOX2 (EPI) and GATA4
069 (PrE) expression. Note, supplementary figure S4 details the same data in raw average cell number format (*i.e.* as
070 presented in Fig. 4, panel d) - bar charts on right) and supplementary tables ST21-ST23 summarise the statistical
071 analysis and individual embryo data.
072
073 **Figure 8: Expression of siRNA resistant recombinant *HA-Wwc2* mRNA rescues *Wwc2* siRNA elicited cell**
074 **number/ division phenotypes. a)** Experimental strategy to assay potential phenotypic rescue of clonal *Wwc2*

expression knockdown by comparing co-microinjection (in one blastomere of 2-cell/E1.5 stage embryos) of GAP43-GFP mRNA (stable plasma membrane fluorescent lineage marker – 'Inj.') with either control siRNA, *Wwc2* siRNA or *Wwc2* siRNA + recombinant *HA-Wwc2* mRNA (containing a N-terminal HA-epitope tag and point mutants conferring siRNA resistance – see supplementary figure S5) and assaying total, outer and inner-cell number at the 32- (E3.5) and >64-cell (late blastocyst/E4.5) stages. **b)** Average clonal contribution ('Inj' vs. 'Non') of outer and ICM cells in control siRNA (blue bars), *Wwc2* siRNA (green bars) and *Wwc2* siRNA + *HA-Wwc2* mRNA (rescue – orange bars) microinjected embryos; errors represent s.e.m. and 2-tailed student t-test derived statistical significance between the three experimental groups (asterisks), or clones ('Inj.' vs 'Non') within a group (double crosses), are highlighted with statistical confidence intervals of $p<0.05$ and $p<0.005$, as denoted by one or two significance markers, respectively. The number of embryos in each experimental group is provided. **c)** Pie charts detailing the overall and clonal distribution of constituent embryo cells between outer and inner-cell populations, plus the incidence of abnormal nuclear morphology (as defined in Fig. 3), in each of the three indicated experimental groups, at the 32-cell/E3.5 early blastocyst (left) and >64-cell/E4.5 late blastocyst (right) stages. Note, the areas of all individual pie chart categories are normalised against those describing the appropriate criteria in the control siRNA condition. **d)** Exemplar confocal z-section micrographs of early/ late blastocysts of the indicated microinjection groups IF stained to detect HA-epitope tag expression (individual greyscale channels plus merged images, in which the anti-HA channel is coloured red and the DAPI cyan). Within the microinjected clone of the *Wwc2* siRNA treated group, white or red asterisks respectively denote characteristic abnormal mitotic or apoptotic cell remnants, whilst in the microinjected clone of the *Wwc2* siRNA + *HA-Wwc2* rescue group, white arrows indicate anti-HA epitope tag signal associated with cell junctions, particular characteristic, in 32-cell (E3.5) stage embryos, as mid-bodies (see also indicated zoomed images); scale bar equals 20μm. Supplementary tables ST24 & ST25 summarise the statistical analysis and individual embryo data used to generate the figure.

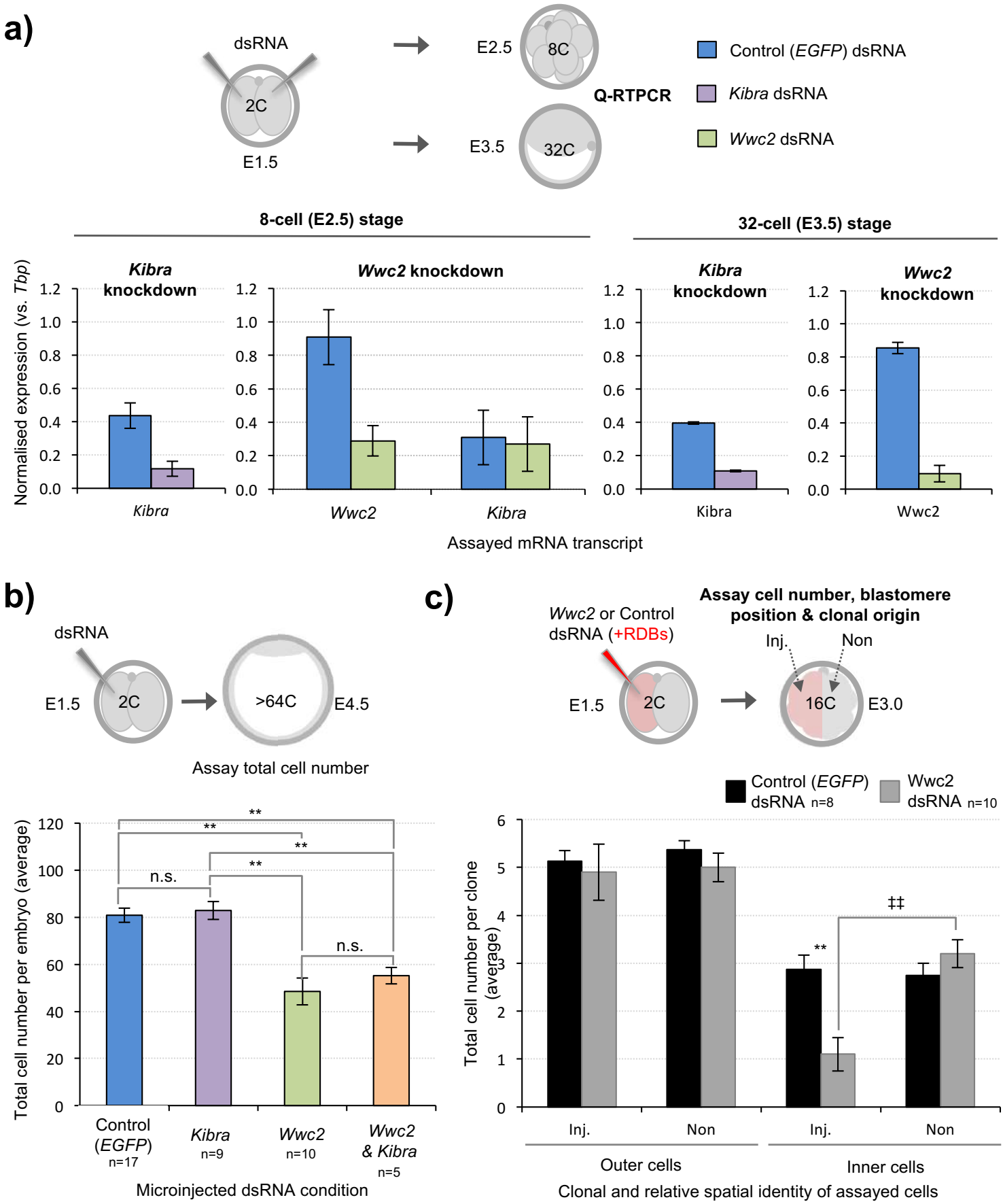
a)
dsRNA
2C
E1.5
E2.5
8C
E3.5
32C
Q-RTPCR
Control (EGFP) dsRNA
Kibra dsRNA
Wwc2 dsRNA
8-cell (E2.5) stage
32-cell (E3.5) stage
Kibra knockdown
Wwc2 knockdown
Normalised expression (vs. Tbp)
Kibra
Wwc2
Assayed mRNA transcript
b)
dsRNA
E1.5
2C
>64C
E4.5
Assay total cell number
Total cell number per embryo (average)
n.s.
**
Control (EGFP) n=17
Kibra n=9
Wwc2 n=10
Wwc2 & Kibra n=5
Microinjected dsRNA condition
c)
Wwc2 or Control dsRNA (+RDBs)
Assay cell number, blastomere position & clonal origin
Inj.
Non
E1.5
2C
16C
E3.0
Control (EGFP) dsRNA n=8
Wwc2 dsRNA n=10
Total cell number per clone (average)
‡‡
Outer cells
Inner cells
Clonal and relative spatial identity of assayed cells

Fig. 1

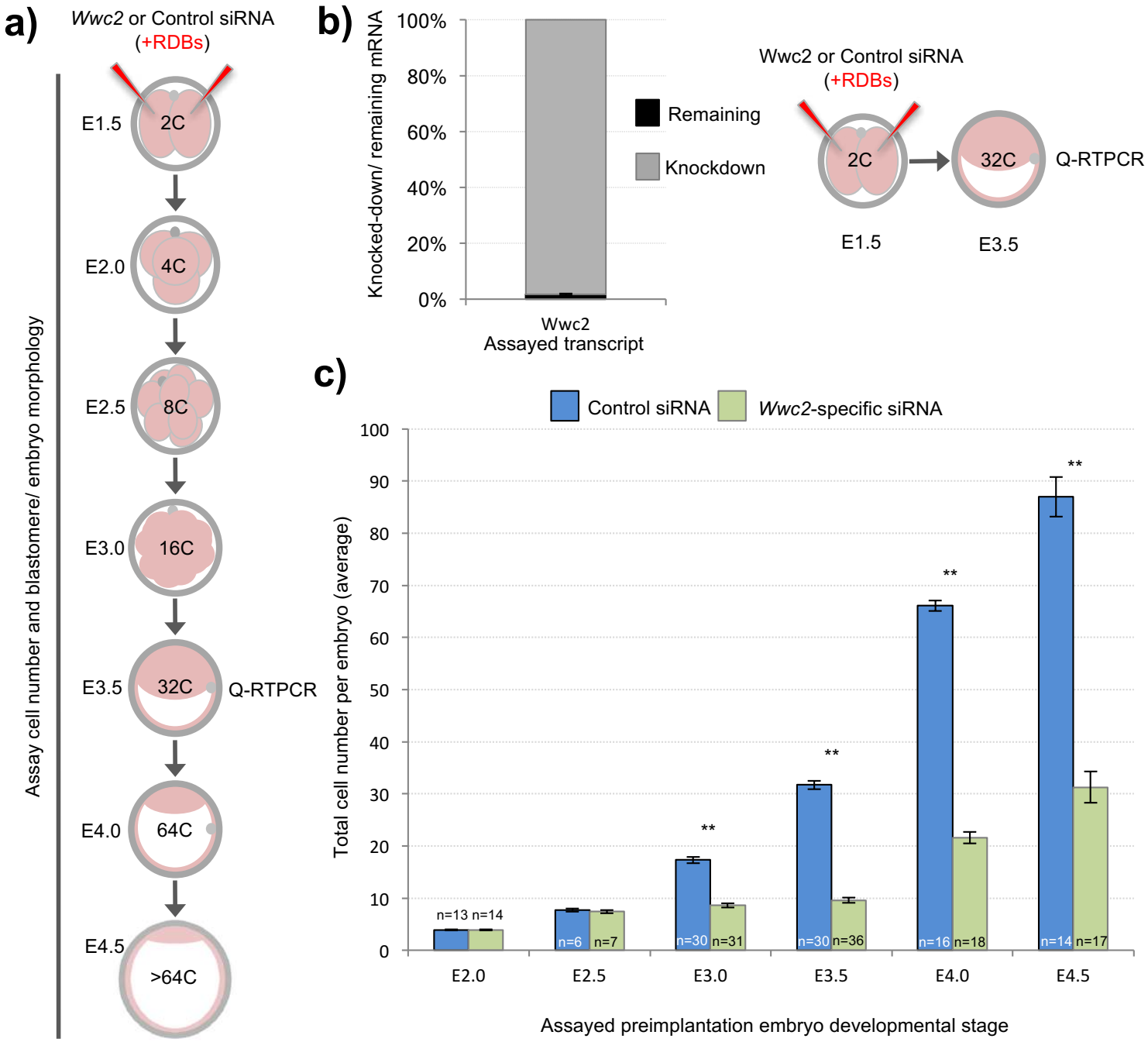
a)
Wwc2 or Control siRNA
(+RDBs)
E1.5
2C
E2.0
4C
E2.5
8C
E3.0
16C
E3.5
32C
Q-RTPCR
E4.0
64C
E4.5
>64C
Assay cell number and blastomere/ embryo morphology
b)
Knocked-down/ remaining mRNA
100%
80%
60%
40%
20%
0%
Remaining
Knockdown
Wwc2
Assayed transcript
Wwc2 or Control siRNA
(+RDBs)
2C
32C
Q-RTPCR
E1.5
E3.5
c)
Control siRNA
Wwc2-specific siRNA
Total cell number per embryo (average)
100
90
80
70
60
50
40
30
20
10
0
**
n=13 n=14
n=6
n=7
n=30
n=31
n=30
n=36
n=16
n=18
n=14
n=17
E2.0
E2.5
E3.0
E3.5
E4.0
E4.5
Assayed preimplantation embryo developmental stage

Fig. 2

Fig. 3

a)

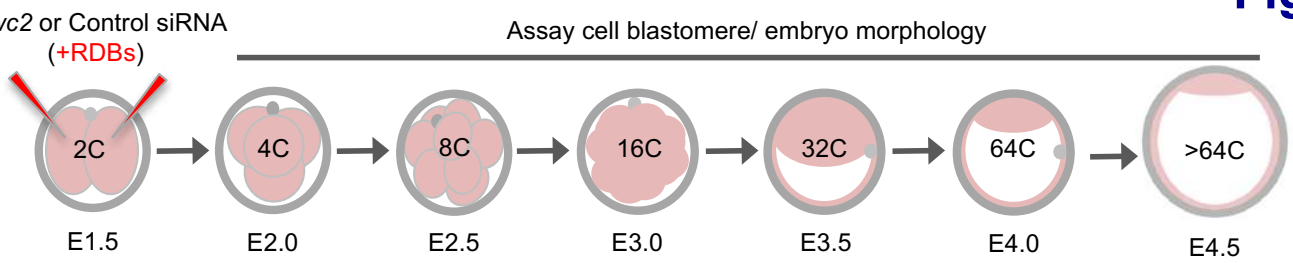

b)

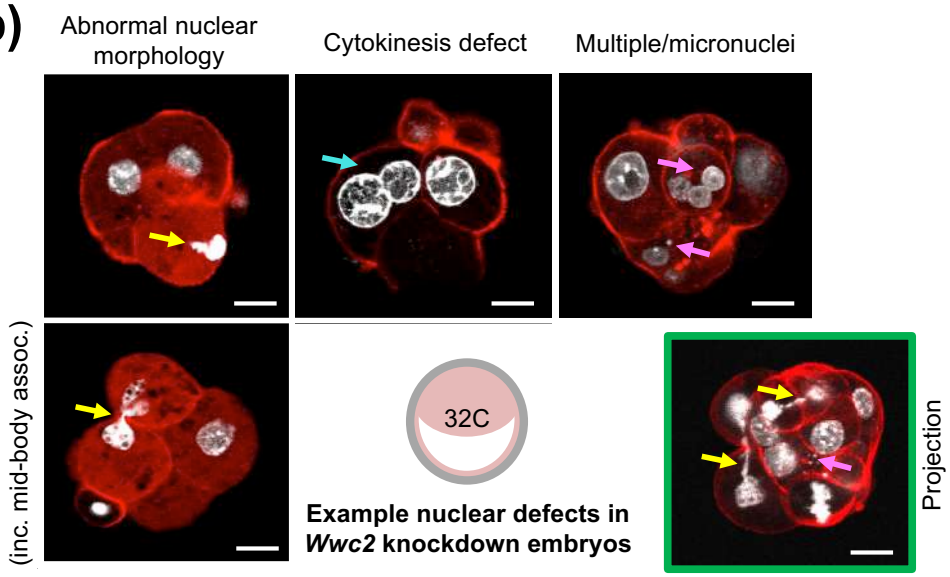

c)

Phenotype		
Presence of multiple/ micronuclei	Observed	
	Unobserved	
Abnormal nuclear morphology	Observed	
	Unobserved	
Cytokinesis defect	Observed	
	Unobserved	
Amalgamated phenotypes	Observed	
	Unobserved	

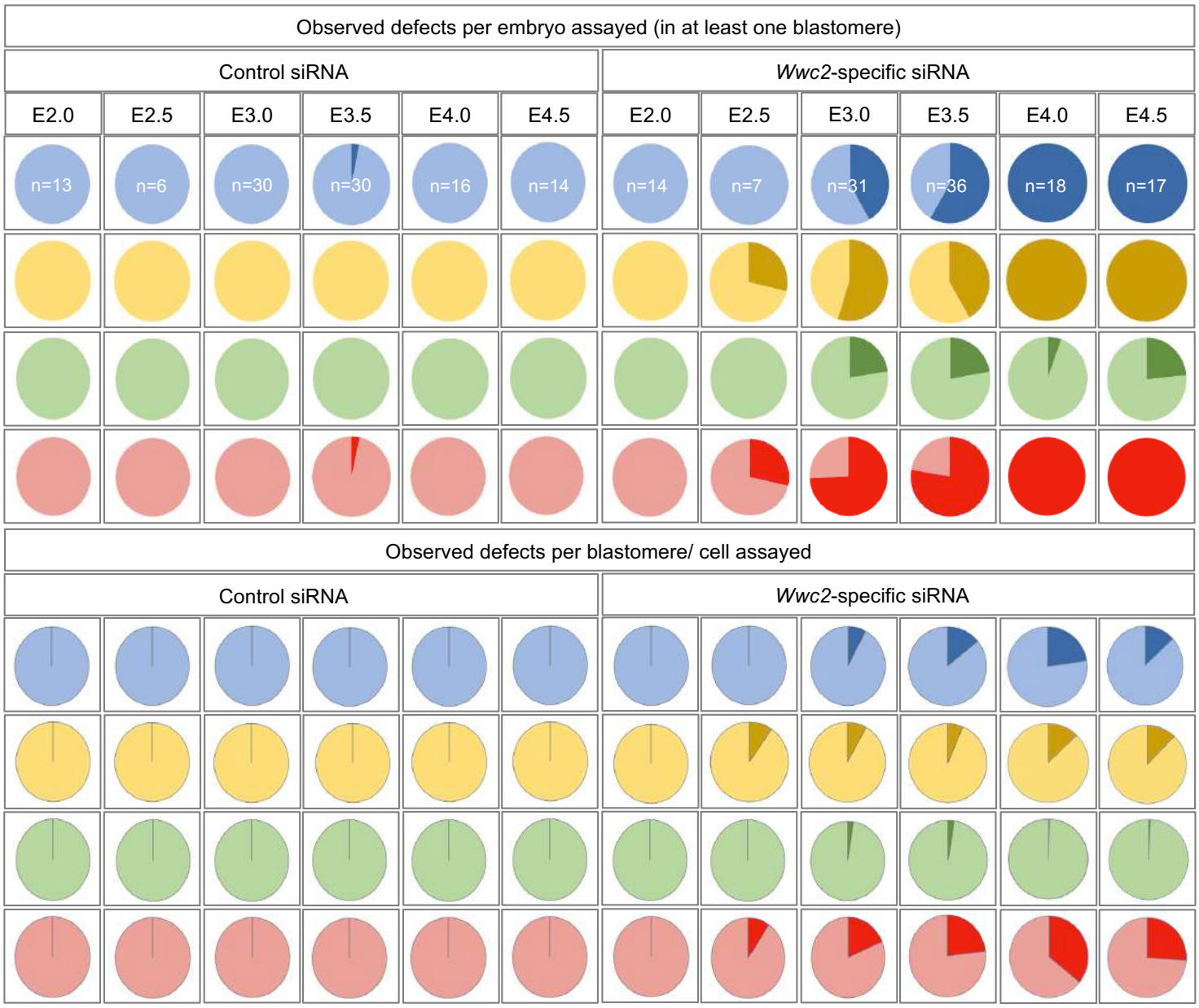

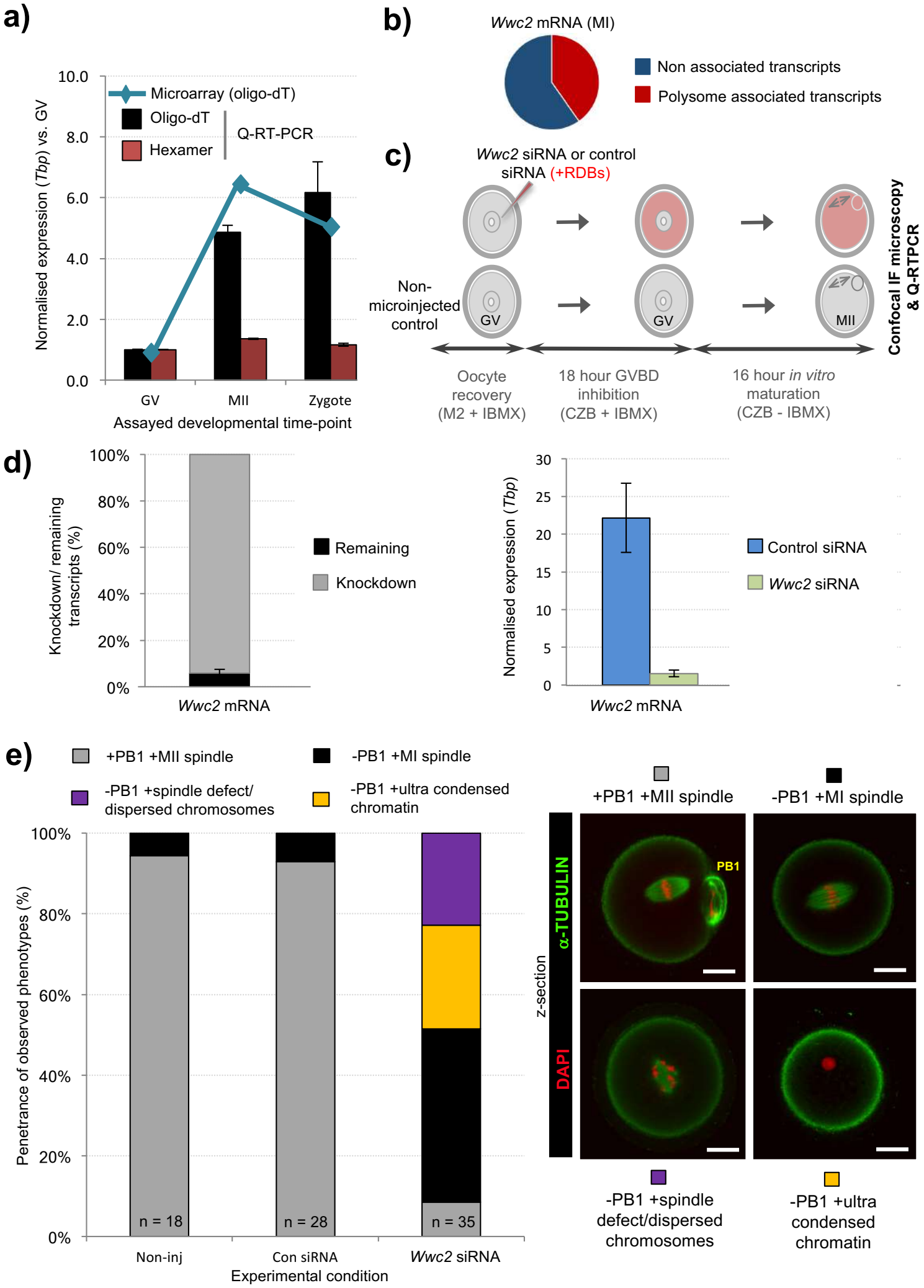
a)
Microarray (oligo-dT)
Oligo-dT
Hexamer
Q-RT-PCR
Normalised expression (Tbp) vs. GV
10.0
8.0
6.0
4.0
2.0
0.0
GV
MII
Zygote
Assayed developmental time-point
b)
Wwc2 mRNA (MI)
Non associated transcripts
Polysome associated transcripts
c)
Wwc2 siRNA or control siRNA (+RDBs)
Non-microinjected control
GV
GV
MII
Confocal IF microscopy & Q-RTPCR
Oocyte recovery (M2 + IBMX)
18 hour GVBD inhibition (CZB + IBMX)
16 hour in vitro maturation (CZB - IBMX)
d)
Knockdown/ remaining transcripts (%)
100%
80%
60%
40%
20%
0%
Remaining
Knockdown
Wwc2 mRNA
Normalised expression (Tbp)
30
25
20
15
10
5
0
Control siRNA
Wwc2 siRNA
Wwc2 mRNA
e)
+PB1 +MII spindle
-PB1 +MI spindle
-PB1 +spindle defect/ dispersed chromosomes
-PB1 +ultra condensed chromatin
Penetrance of observed phenotypes (%)
100%
80%
60%
40%
20%
0%
n = 18
n = 28
n = 35
Non-inj
Con siRNA
Wwc2 siRNA
Experimental condition
+PB1 +MII spindle
-PB1 +MI spindle
α-TUBULIN
DAPI
z-section
PB1
-PB1 +spindle defect/dispersed chromosomes
-PB1 +ultra condensed chromatin

Fig. 4

Fig. 5

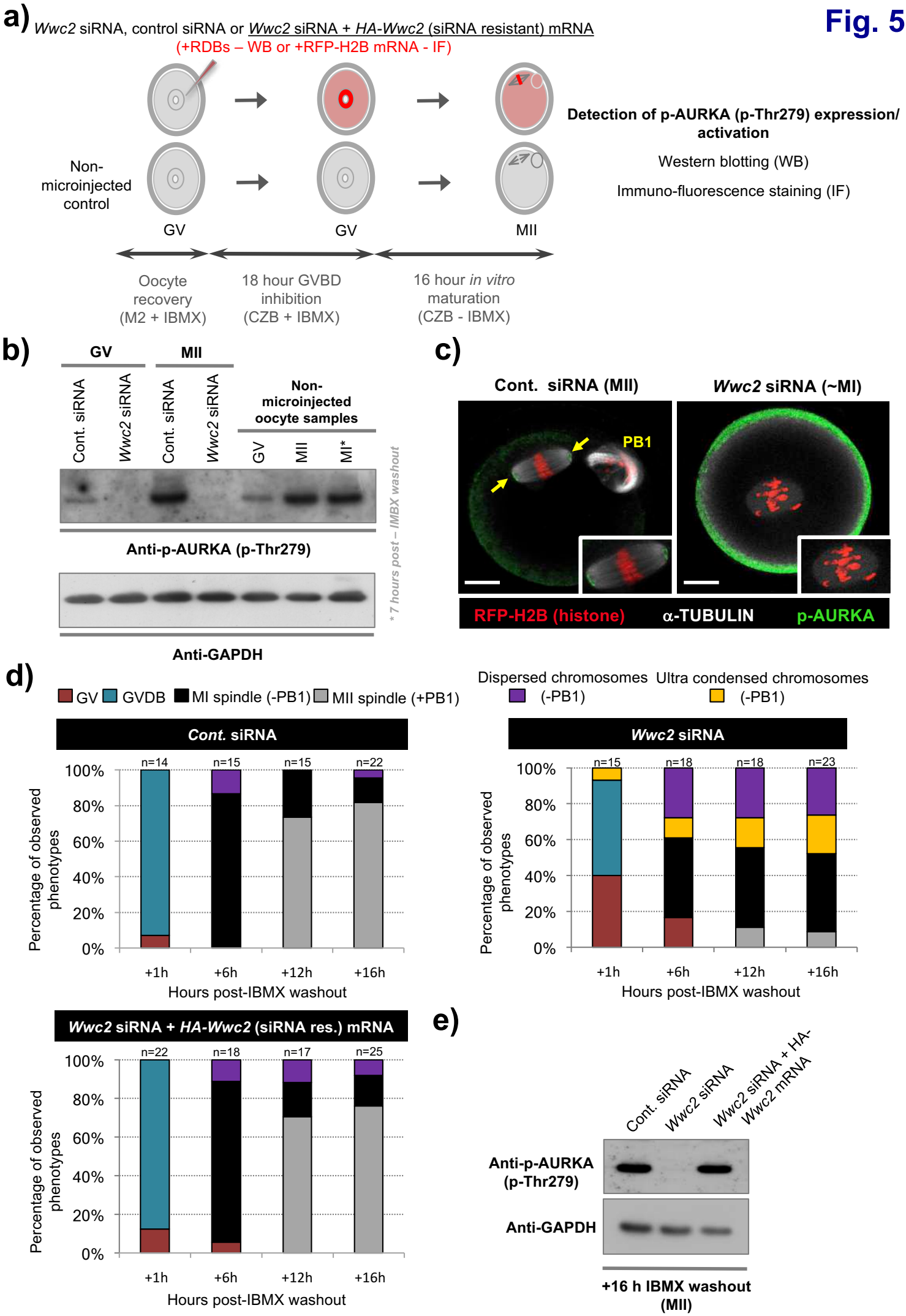
a)
Wwc2 siRNA, control siRNA or Wwc2 siRNA + HA-Wwc2 (siRNA resistant) mRNA
(+RDBs – WB or +RFP-H2B mRNA - IF)
Non-microinjected control
GV
GV
MII
Detection of p-AURKA (p-Thr279) expression/ activation
Western blotting (WB)
Immuno-fluorescence staining (IF)
Oocyte recovery (M2 + IBMX)
18 hour GVBD inhibition (CZB + IBMX)
16 hour in vitro maturation (CZB - IBMX)
b)
GV
MII
Cont. siRNA
Wwc2 siRNA
Cont. siRNA
Wwc2 siRNA
Non-microinjected oocyte samples
GV
MII
MI*
Anti-p-AURKA (p-Thr279)
Anti-GAPDH
* 7 hours post – IMBX washout
c)
Cont. siRNA (MII)
Wwc2 siRNA (~MI)
PB1
RFP-H2B (histone)
α-TUBULIN
p-AURKA
d)
GV
GVDB
MI spindle (-PB1)
MII spindle (+PB1)
Dispersed chromosomes (-PB1)
Ultra condensed chromosomes (-PB1)
Cont. siRNA
Wwc2 siRNA
Wwc2 siRNA + HA-Wwc2 (siRNA res.) mRNA
Percentage of observed phenotypes
100%
80%
60%
40%
20%
0%
n=14
n=15
n=15
n=22
n=15
n=18
n=18
n=23
n=22
n=18
n=17
n=25
+1h
+6h
+12h
+16h
Hours post-IBMX washout
e)
Cont. siRNA
Wwc2 siRNA
Wwc2 siRNA + HA-Wwc2 mRNA
Anti-p-AURKA (p-Thr279)
Anti-GAPDH
+16 h IBMX washout (MII)

Fig. 6

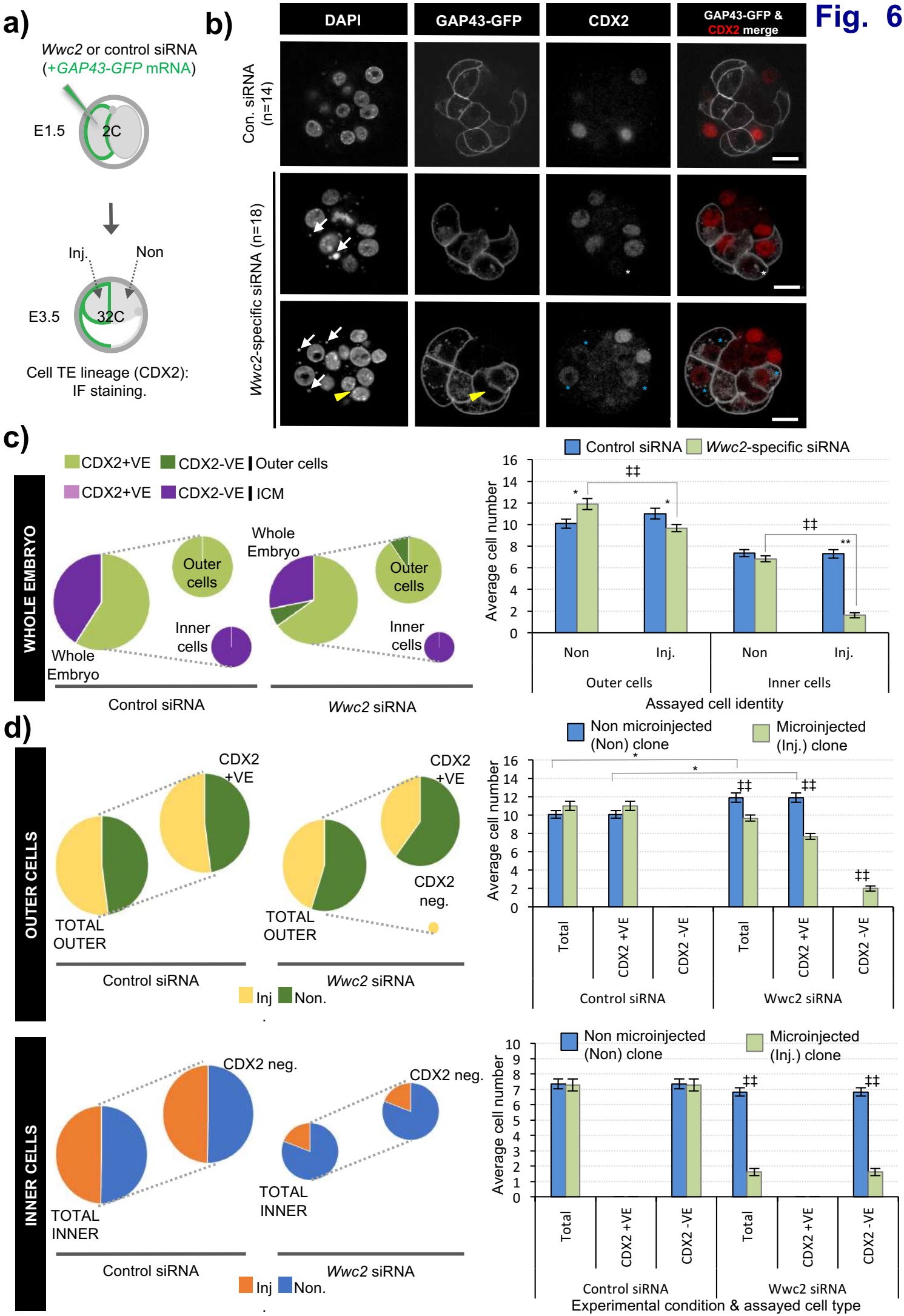
a)
Wwc2 or control siRNA
(+GAP43-GFP mRNA)
E1.5
2C
Inj.
Non
E3.5
32C
Cell TE lineage (CDX2):
IF staining.
b)
DAPI
GAP43-GFP
CDX2
GAP43-GFP & CDX2 merge
Con. siRNA (n=14)
Wwc2-specific siRNA (n=18)
c)
CDX2+VE
CDX2-VE
Outer cells
CDX2+VE
CDX2-VE
ICM
WHOLE EMBRYO
Whole Embryo
Outer cells
Inner cells
Control siRNA
Wwc2 siRNA
Control siRNA
Wwc2-specific siRNA
Average cell number
Non
Inj.
Outer cells
Inner cells
Assayed cell identity
d)
OUTER CELLS
CDX2 +VE
TOTAL OUTER
CDX2 neg.
Control siRNA
Wwc2 siRNA
Inj
Non.
Non microinjected (Non) clone
Microinjected (Inj.) clone
Total
CDX2 +VE
CDX2 -VE
Control siRNA
Wwc2 siRNA
INNER CELLS
CDX2 neg.
TOTAL INNER
Experimental condition & assayed cell type

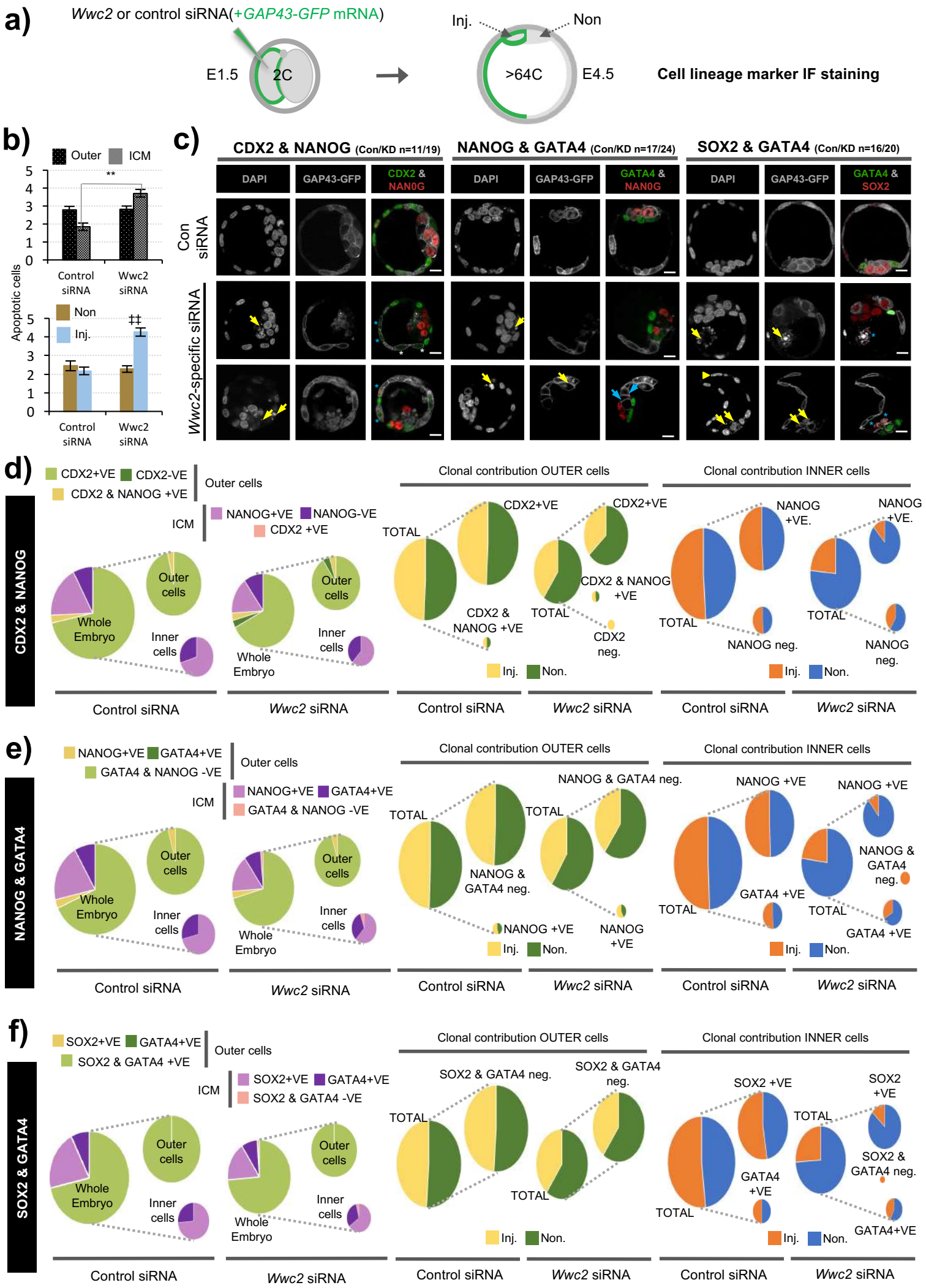
a)
Wwc2 or control siRNA(+GAP43-GFP mRNA)
E1.5
2C
Inj.
Non
>64C
E4.5
Cell lineage marker IF staining
b)
Outer
ICM
Apoptotic cells
Control siRNA
Wwc2 siRNA
Non
Inj.
c)
CDX2 & NANOG (Con/KD n=11/19)
NANOG & GATA4 (Con/KD n=17/24)
SOX2 & GATA4 (Con/KD n=16/20)
DAPI
GAP43-GFP
CDX2 & NANOG
GATA4 & NANOG
GATA4 & SOX2
Con siRNA
Wwc2-specific siRNA
d)
CDX2 & NANOG
CDX2+VE
CDX2-VE
CDX2 & NANOG +VE
Outer cells
ICM
NANOG+VE
NANOG-VE
CDX2 +VE
Clonal contribution OUTER cells
Clonal contribution INNER cells
Whole Embryo
Inner cells
TOTAL
CDX2 & NANOG +VE
CDX2 neg.
NANOG +VE.
NANOG neg.
Inj.
Non.
Control siRNA
Wwc2 siRNA
e)
NANOG & GATA4
NANOG+VE
GATA4+VE
GATA4 & NANOG -VE
NANOG & GATA4 neg.
GATA4 +VE
f)
SOX2 & GATA4
SOX2+VE
GATA4+VE
SOX2 & GATA4 +VE
SOX2 & GATA4 -VE
SOX2 & GATA4 neg.
SOX2 +VE
SOX2 +VE
GATA4 +VE
GATA4+VE

Fig. 7

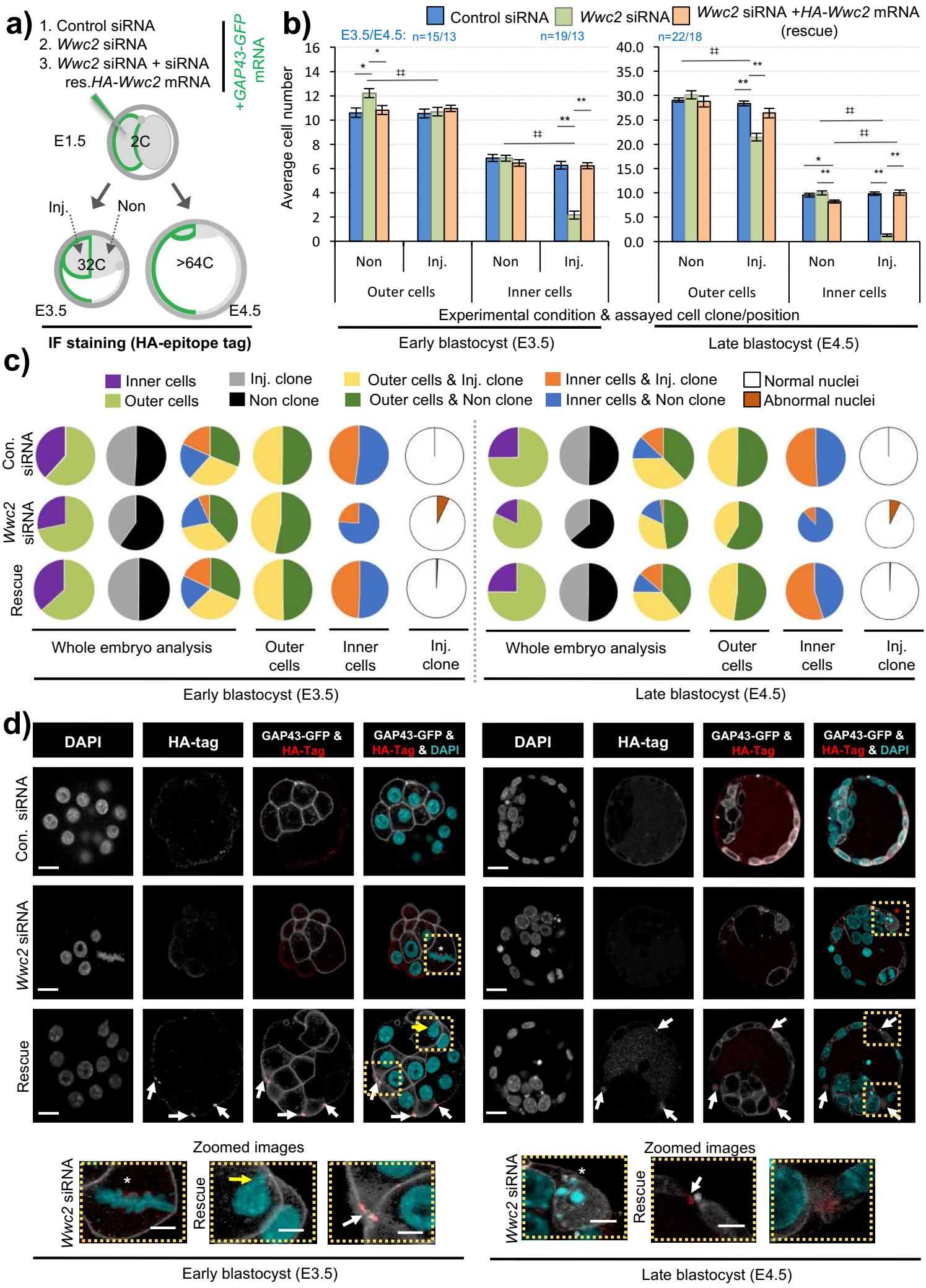
a)
1. Control siRNA
2. Wwc2 siRNA
3. Wwc2 siRNA + siRNA res.HA-Wwc2 mRNA
+GAP43-GFP mRNA
E1.5
2C
Inj.
Non
32C
>64C
E3.5
E4.5
IF staining (HA-epitope tag)
b)
Control siRNA
Wwc2 siRNA
Wwc2 siRNA +HA-Wwc2 mRNA (rescue)
E3.5/E4.5: n=15/13
n=19/13
n=22/18
Average cell number
Non
Inj.
Outer cells
Inner cells
Experimental condition & assayed cell clone/position
Early blastocyst (E3.5)
Late blastocyst (E4.5)
c)
Inner cells
Outer cells
Inj. clone
Non clone
Outer cells & Inj. clone
Outer cells & Non clone
Inner cells & Inj. clone
Inner cells & Non clone
Normal nuclei
Abnormal nuclei
Con. siRNA
Wwc2 siRNA
Rescue
Whole embryo analysis
Outer cells
Inner cells
Inj. clone
Early blastocyst (E3.5)
Late blastocyst (E4.5)
d)
DAPI
HA-tag
GAP43-GFP & HA-Tag
GAP43-GFP & HA-Tag & DAPI
Con. siRNA
Wwc2 siRNA
Rescue
Zoomed images
Wwc2 siRNA
Rescue
Early blastocyst (E3.5)
Late blastocyst (E4.5)

Fig. 8